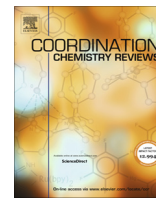




Since January 2020 Elsevier has created a COVID-19 resource centre with free information in English and Mandarin on the novel coronavirus COVID-19. The COVID-19 resource centre is hosted on Elsevier Connect, the company's public news and information website.

Elsevier hereby grants permission to make all its COVID-19-related research that is available on the COVID-19 resource centre - including this research content - immediately available in PubMed Central and other publicly funded repositories, such as the WHO COVID database with rights for unrestricted research re-use and analyses in any form or by any means with acknowledgement of the original source. These permissions are granted for free by Elsevier for as long as the COVID-19 resource centre remains active.



## Review

# Heteroleptic copper phenanthroline complexes in motion: From stand-alone devices to multi-component machinery

Abir Goswami, Michael Schmittel\*

Center of Micro- and Nanochemistry and Engineering, Organische Chemie I, Universität Siegen, Adolf-Reichwein-Str. 2, D-57068 Siegen, Germany

## ARTICLE INFO

## Article history:

Received 31 May 2018

Received in revised form 7 July 2018

Accepted 13 August 2018

Available online 5 September 2018

## Keywords:

Copper

Phenanthroline

Diimine

Kinetics

Rate

Molecular machines

Devices

Switches

## ABSTRACT

Two and a half decades of copper phenanthroline-based switches, devices and machines have illustrated the rich dynamic nature of these metal complexes. With an emphasis on the metal-ligand dissociation as the rate-determining step the present review summarizes not only spectacular examples of machinery, but also highlights rate data collected during a variety of investigations. Copper-ligand exchange reactions are mostly triggered by redox processes, addition of metal ions or addition of ligands. While the rate data spread over >8 orders of magnitude, individual effects of solvent, steric bulk, flexibility,  $\sigma$ -basicity and the trajectory (intra- vs. intermolecular dissociation) have large impact. Unfortunately, in many cases the exact mechanism in the rate-determining step (nucleophile-induced vs. monomolecular metal-ligand dissociation) has not been determined, suggesting to invest further efforts in the physical (in)organic chemistry of such coordination-driven systems.

© 2018 Elsevier B.V. All rights reserved.

## Contents

1. Introduction	479
2. Selected examples of stand-alone switches, devices and machines	479
2.1. Topological control	479
2.2. Nanomechanical switches	482
2.3. Supramolecular switches, devices and machines	486
2.3.1. Three-component machines	486
2.3.2. Four-component switches and machines	489
3. Catalytic and networked multi-component machinery	491
3.1. Self-sorting and multi-component machinery	491
3.2. Catalytic machinery	491
3.3. Networked catalytic machinery	492
3.3.1. Double-NetState nine-component catalytic machinery	493
3.3.2. Double-NetState nine-component machinery: rotation and catalysis	493
4. Kinetic factors	494
4.1. Kinetics in mononuclear copper(I) phenanthroline and diimine complexes	494
4.2. Topologically controlled switches, devices and machines	496
4.3. Nanomechanical switches	500
4.4. Supramolecular machines	501
4.5. Conclusions on kinetic data	503
5. Conclusion	503
Acknowledgments	503
References	504

\* Corresponding author.

E-mail address: [schmittel@chemie.uni-siegen.de](mailto:schmittel@chemie.uni-siegen.de) (M. Schmittel).

## 1. Introduction

This review focuses on heteroleptic copper(I) phenanthroline and some selected diimine complexes because of their eminent role in coordination-based molecular machines. The reason for this exceptional standing is three-fold: (a) among the large amount of thermodynamically strong metal complexes, the copper-phenanthroline interaction is highly labile, thus allowing motion-based devices via rate-determining metal-ligand dissociation. (b) Moreover, several strategies are known (*vide infra*) that allow the clean preparation of heteroleptic complexes, which is a key prerequisite for structurally diverse molecular machinery. (c) Since NMR characterization is imperative, the diamagnetic nature is another factor suggesting use of copper(I) ions. We are grateful to Jean-Pierre Sauvage for initiating the field and providing continued inspiration over several decades through the demonstration of fascinating copper(I)-based catenane and rotaxane machines [1].

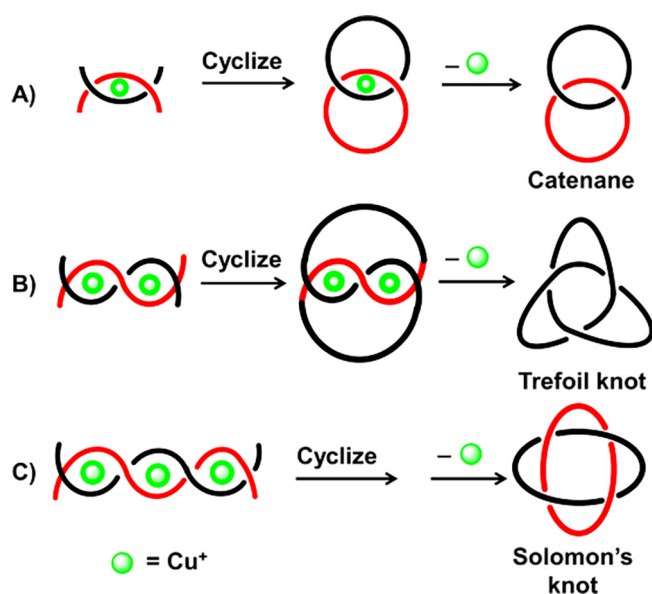


Fig. 1. Strategies for making mechanically interlocked molecules.

As distinct states of switches, devices and machines sometimes go along with major constitutional change(s) we will use different numbers for the very same multifunctional ligand & metal ion ensemble depending on the connected binding site(s). The  $N_{\text{phen}} \rightarrow$  copper(I) phenanthroline interaction (with phen representing any phenanthroline) has been exploited in a variety of mechanically interlocked molecules, nanoswitches and nanorotors in the past decades [1]. We will denote this general complexation motif as  $[\text{Cu}(\text{phen})_2]^+$ , with the superscript expression in brackets describing the coordination number of the metal ion.

## 2. Selected examples of stand-alone switches, devices and machines

### 2.1. Topological control

Interlocked structures, in particular rotaxanes or catenanes, are ideally suited for designing molecular machines due to the fact that motion is possible without dissociation of components. Moreover their preparation is facilitated by the template effect [2] as impressively demonstrated by Sauvage in 1983. Over the years this method has developed into a highly successful strategy for preparing copper(I) phenanthroline-based catenanes (Fig. 1), and several other types of interlocked molecule, such as rotaxanes [3], molecular knots [4] etc., equally became accessible by this approach. In the 80s and early 90s, control and variation of the topological outcome was a main focus of Sauvage's work [5]. In particular for the fabrication of knots, a series of fascinating designs were developed, but throughout this work the lability of copper(I) phenanthroline complexes was not used for machine-type of motions, rather only to remove the copper for preparing the metal-free structures.

Use of the intrinsic lability of the  $[\text{Cu}(\text{phen})(\text{L})]^+$  complex ( $\text{L} =$  any ligand) for machine-type function was elaborated by Sauvage in 1994 [6]. The electrochemically triggered swinging in the  $[\text{Cu}(\text{phen})_2]^+$ -based [2]-catenane  $[\text{Cu}(\mathbf{1})]^+$  (Fig. 2) relies on the different coordination preferences of copper(I) vs. copper(II) and follows a four-step mechanism. First, the stable tetracoordinated copper(I) complex  $[\text{Cu}(\mathbf{1})]^+$  is oxidized to the intermediate tetrahedral species  $[\text{Cu}(\mathbf{1})]^{2+}$ . However, since this complex contains the copper (II) ion in a thermodynamically less favorable tetracoordination, it

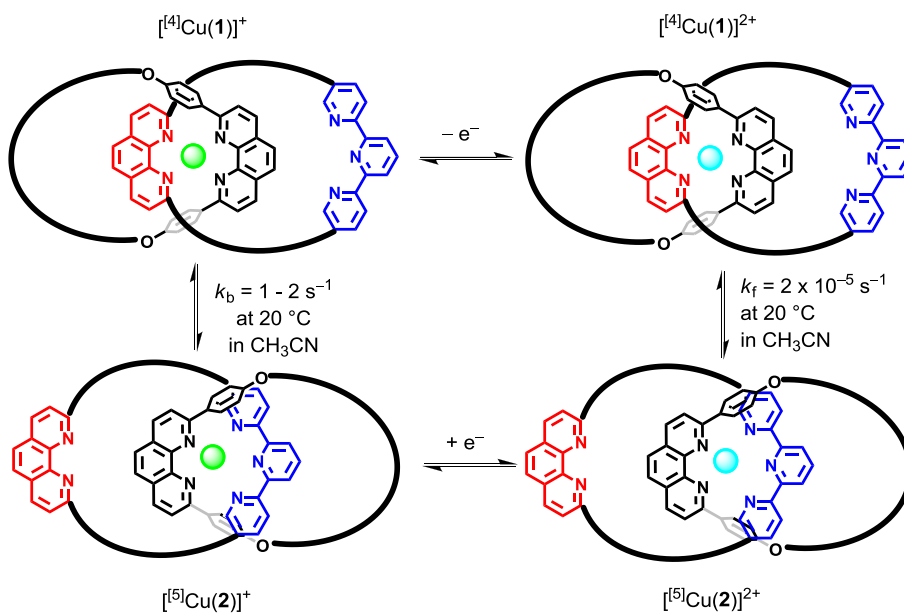


Fig. 2. Electrochemically triggered dynamics in an [2]-catenane [6].

undergoes a full reorganization to afford the stable pentacoordinate complex  $[\text{Cu}(\text{phen})_2]^{2+}$ . Upon reduction, the pentacoordinate  $[\text{Cu}(\text{phen})(\text{terpy})]^{+2+}$  is formed as a transient state. Now the copper(I) center is embedded in a thermodynamically unfavorable coordination setting and thus undergoes a structural change that regenerates the initial complex  $[\text{Cu}(\text{phen})]^{+}$ . Notably, the rate constant for the forward mechanical motion is far less than that for the backward process [6].

While catenanes undergo rotation of one ring with regard to the other, the analogous  $[\text{Cu}(\text{phen})_2]^{+2+} \rightleftharpoons [\text{Cu}(\text{phen})(\text{terpy})]^{+2+}$  reorganization was used in rotaxanes for either gliding along the thread, i.e. in a linear motor (shuttle), or for pirouetting about the axis, i.e. in a rotor (Fig. 3). Copper(I) phenanthroline-based rotaxanes have been made using an analogous template approach and both motions, shuttling and pirouetting, have been demonstrated by several groups [7–11]. The first example, with the macrocycle moving along the thread [12], was reported by Sauvage in 1997, while the pirouetting rotaxane was developed in 1999 [13]. Pirouetting of a macrocycle around its axle upon oxidation of copper(I) proved to be a faster process in general than the translation of a macrocycle along a molecular thread.

An advanced machinery based on dimeric transition metal-based [2]rotaxanes, so called molecular muscles, was first introduced in 2000 [14]. The clever design of this landmark develop-

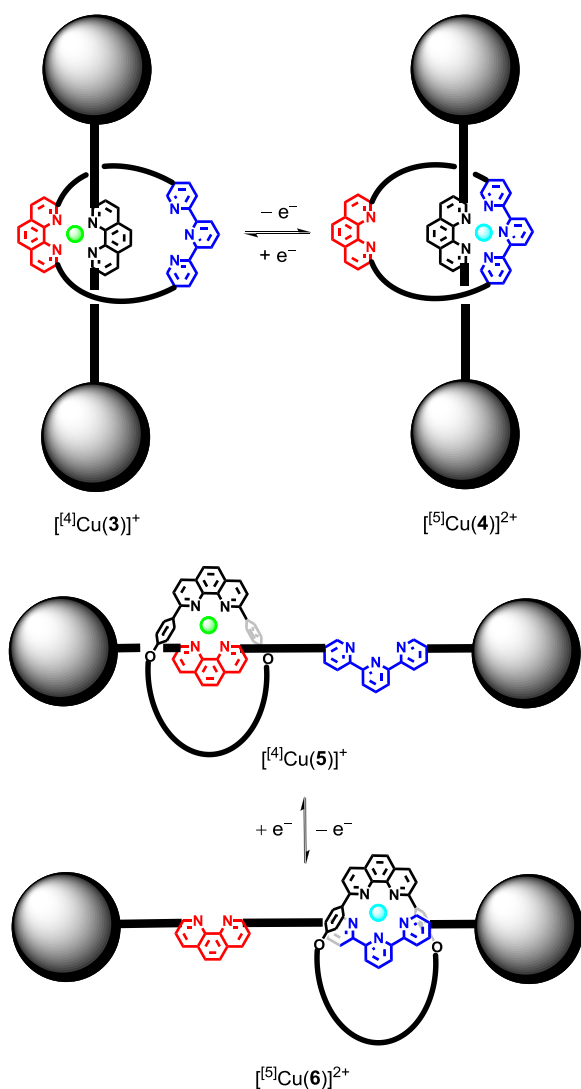


Fig. 3. Pirouetting of a macrocycle around its axle upon oxidation of copper(I) (top), and translation of a macrocycle along a molecular thread (bottom) [12,13].

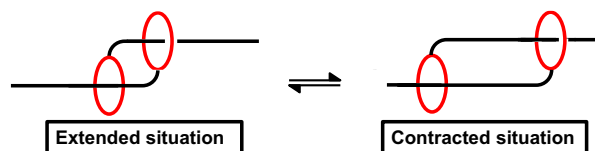


Fig. 4. Conceptual linkage used by Sauvage in molecular muscles.

ment by Sauvage is based on two identical parts that glide along each other under the action of a chemical signal (Fig. 4). The resultant contraction/extension mimics the mode of operation of a muscle. Capitalizing on the switching behavior in simple catenane- and rotaxane-based switches, copper(I) ions were used to construct the doubly threaded [2]rotaxane dimer  $[\text{Cu}_2(\text{7})_2]^{2+}$  that is able to ingest two more metal ions, either in a four- or five-coordinate geometry (Fig. 5). As redox initiation, i.e.  $\text{Cu}^+ \rightleftharpoons \text{Cu}^{2+}$ , failed to initiate the desired motion, the rearrangement was induced by metal exchange as shown schematically in Fig. 5. Since copper(I) prefers the four-coordinate complexation in  $[\text{Cu}_2(\text{7})_2]^{2+}$ , the endotopic phenanthroline in the macrocycle of the first unit **7** is bound via copper(I) to the non-macrocyclic phenanthroline unit of the opposing second **7**. This binding mode corresponds to an extended geometry (Fig. 5). Upon addition of zinc(II) followed by removal of copper(I) the five-coordinate situation prevails in  $[\text{Zn}_2(\text{8})_2]^{4+}$  that corresponds to the interaction of both zinc ions with one endotopic phenanthroline and one open-chain terpyridine (terpy) unit of the opposing unit. This state corresponds to a contracted geometry (Fig. 5). The change in length due to contraction/extension is roughly the same as that found in natural muscles ( $\approx 27\%$ ). This amazing case constitutes the first example of a unimolecular linear array that is able to elongate and contract under the action of a given chemical input, later followed by other cases [15], but unfortunately the authors did not undertake any rate measurements of the contraction/extension process.

So far, the overall nanomechanical motion has been successfully instigated by cleaving coordinative bonds, but in detail the mechanistic scenario depends decisively on the mode of initiation. For instance, when using redox actuation, typically the copper(I) center in the rotaxane is oxidized (Fig. 6, left), with the consequence that the  $[\text{Cu}(\text{phen})(\widehat{\text{LL}})]^{2+}$  unit ( $\widehat{\text{LL}}$  = any chelate ligand) is cleaved to  $[\text{Cu}(\text{phen})]^{2+}$  and  $\widehat{\text{LL}}$ , and the macrocyclic  $[\text{Cu}(\text{phen})]^{2+}$  shifts to another coordination site on the thread with higher thermodynamic stability. Dissociation or nucleophile-assisted dissociation of  $\widehat{\text{LL}}$  will constitute the rate-determining step. In case of chemical input(s) the situation is quite different. The added metal ion will first coordinate to the vacant tridentate site of the thread, then the macrocycle will move without metal ion to the new coordination site (Fig. 6, middle). Here, the coordinative bond cleavage has to take place on the stage of  $[\text{Cu}(\text{phen})(\widehat{\text{LL}})]^{+}$ . Another possibility arises when the demetalation is initiated prior to addition of the divalent metal (Fig. 6, right). Here the demetalation is rate-determining. Thus depending on the scenario the rate-determining steps are quite distinct and so are the activation parameters. However, as we detail later in Chapter 4.1, all these processes are usually accelerated in the presence of nucleophiles which help to dissociate the departing ligand.

A conceptually atypical dynamic process at copper phenanthroline complexes was designed by Sauvage and his team with an electrochemically triggered wing-flapping motion [16], based on a process studied originally in copper helicates [17]. This motion

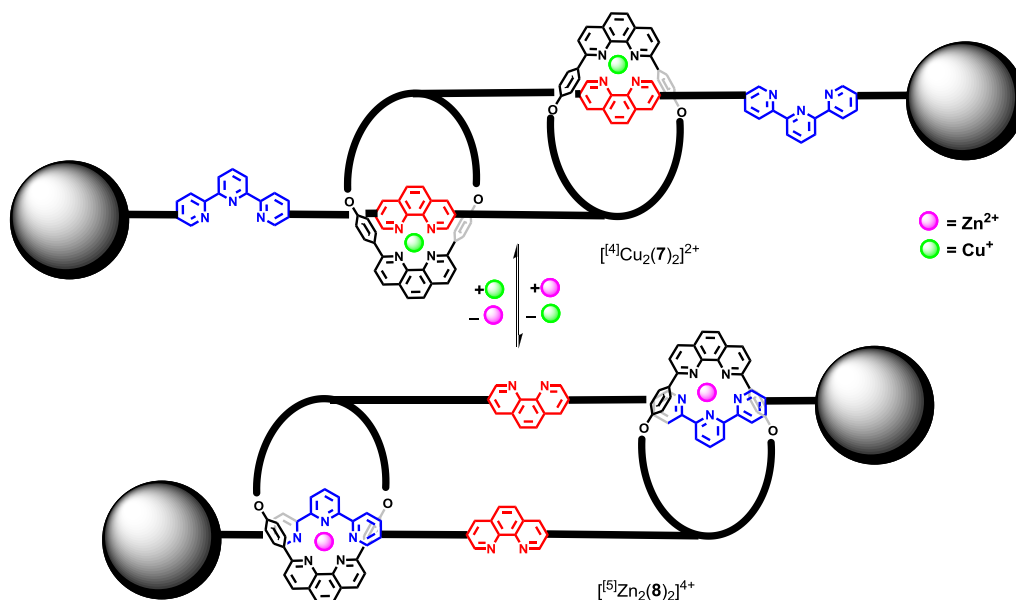


Fig. 5. [2]rotaxanes dimers used as a chemically triggered molecular muscle [14].

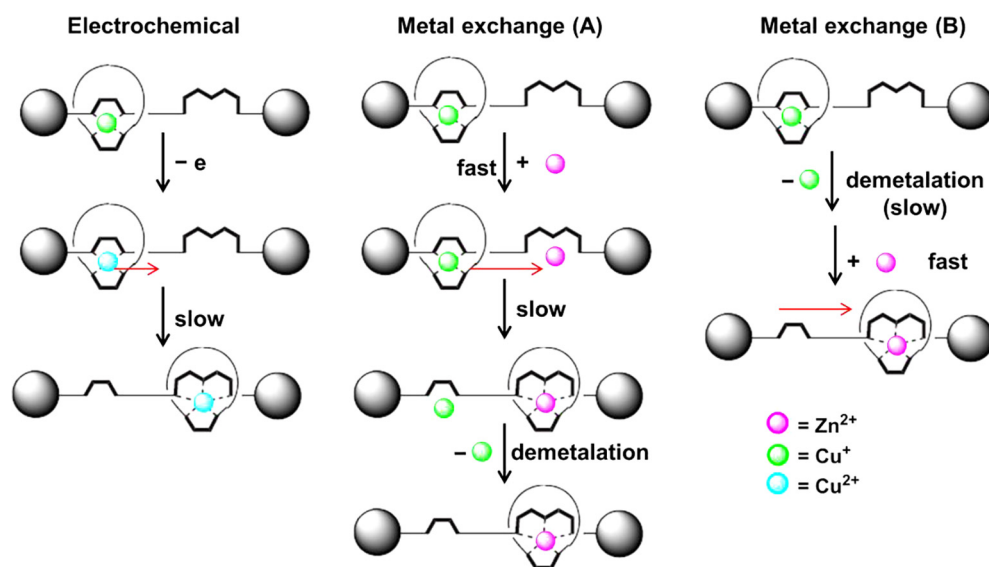


Fig. 6. Mechanisms for mechanical motion in rotaxanes in response to different stimuli.

in [3]rotaxane  $[\text{Cu}_2(\mathbf{9})(\mathbf{10})_2]^{2+}$  is much faster than a similar one when it is based on metal exchange (Fig. 7). In the initial state, both copper(I) ions are tetracoordinated despite the availability of five nitrogen donor atoms from the nearby bipyridine (bipy) and terpyridine-like (terpy) binding sites. In contrast, when the metal centers become divalent, such as in copper(II) or zinc(II), the triazole groups are additionally bound to the metal ions (Fig. 7) to enable pentacoordination. Interconversion between the two coordination environments entails a notable angle change at both triazole rings, which is reminiscent of a wing-flapping movement similar to that of birds. The mechanistic scenario is different for both modes of actuation. When zinc(II) is added to  $[\text{Cu}_2(\mathbf{9})(\mathbf{10})_2]^{2+}$ , it has to displace the copper(I), which means that all four  $N \rightarrow \text{copper(I)}$  bonds have to break on the way to  $[\text{Zn}_2(\mathbf{9})(\mathbf{10})_2]^{4+}$ . In contrast, electrochemical actuation does not require any (in the oxidation step) or only one coordination bond (in the reduction step) to be broken. Therefore this movement is one of the fastest

motions induced in copper-diimine complexes of interlocked systems.

A figure-of-eight type of molecular machine-prototype that could be used as novel element in muscle-like dynamic systems has been established by the Sauvage group recently [18]. The authors have prepared this structure as a large ring containing alternately two bidentate (phen) and tridentate (terpy) ligand sites (Fig. 8). Based on the coordination preference of metal ions, the macrocyclic ligand can be reversibly toggled between two states by applying electrochemical or chemical stimuli. Treatment of **11** with copper(I) ions furnished an intramolecular  $[\text{Cu}(\text{phen})_2]^+$  complex,  $[\text{Cu}(\mathbf{11})]^+$ . In contrast, removal of copper(I) and addition of iron(II) ions afforded the octahedral bisterpyridine complex  $[\text{Fe}(\text{terpy})_2]^{2+}$ ,  $[\text{Fe}(\mathbf{12})]^{2+}$ . This exchange entails major geometric changes. The height of complex  $[\text{Fe}(\mathbf{12})]^{2+}$  measured as distance at the tridentate ligands is only  $\sim 11$  Å, whereas it is almost three times larger for  $[\text{Cu}(\mathbf{11})]^+$ . Importantly, the two figure-of-eight



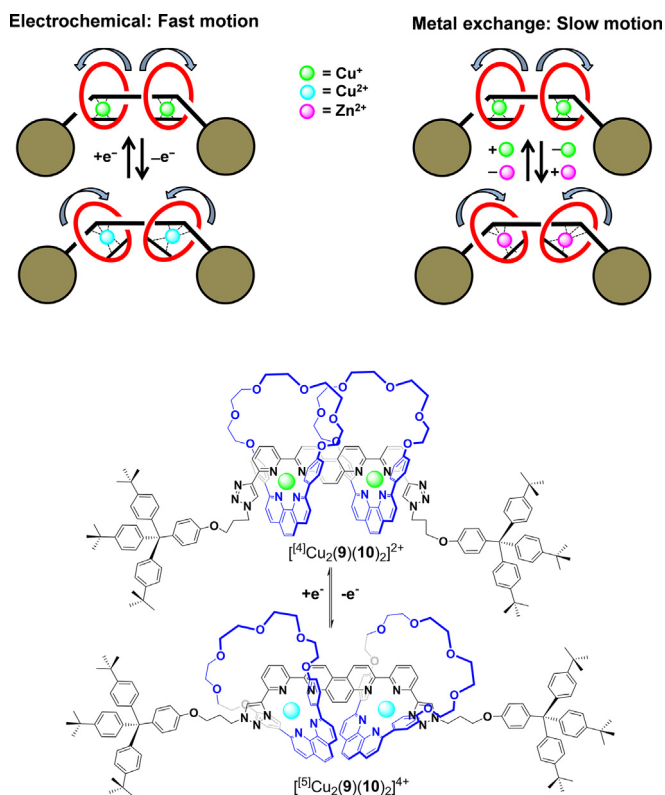


Fig. 7. Electrochemically and chemically triggered flipping motion at two rings [16].

structures of  $[\text{Cu}(\mathbf{11})]^{+2+}$  can be reversibly toggled by applying electrochemical stimuli and thus be of convenient use for the contraction/extension of oligomers or polymers. The oxidized species  $[\text{Cu}(\mathbf{11})]^{2+}$  rearranged within several tens of seconds to the hexa-coordinated copper complex  $[\text{Cu}(\mathbf{12})]^{2+}$ . A full kinetic investigation, however, was not undertaken.

Molecular machines, able to perform controllable mechanical motions, are in principle ideally suited for the design of stand-

alone devices with mechanical, electronic, and sensing functions. While solution-based systems have been extensively studied over the past decade(s), interfacing them with the macroscopic world would enormously expand their potential for applications. For this purpose, catenanes and rotaxanes have been attached to surfaces revealing some promising properties [19]. However the device, once deposited on solid surface, is often far less mobile than the corresponding system in solution. The group of Sauvage tried to resolve the kinetics of  $N, N_{\text{LL}} \rightarrow ([\text{Cu}(\text{phen})]^{+2+})$  bond cleavage of surface-bound rotaxanes and catenanes (Fig. 9) [20,21]. Unfortunately, e.g. in  $[\text{Cu}(\mathbf{14})(\mathbf{15})]^+$ , no redox triggered rotary motion was detected, which reflects the kinetic and thermodynamic differences of mechanical motions of solution vs surface-bound systems (see Fig. 9).

## 2.2. Nanomechanical switches

Other than phenanthroline, the bipyridine ligand leads to weaker metal ion complexes, but additionally has the advantage of conformational flexibility. Early conformational switches based on the *syn* vs. *anti* orientation of extended bipyridines [22] thus have been elegantly exploited for allosteric receptors, originally by Beer [23] and later by Lützen et al. [24,25], in both cases by (de-)complexing the bipyridine in a heteroleptic manner to a metal ion fragment. Intramolecular complexation between two bipyridine sites was utilized by Koert et al. for conformational signal transduction [26], by Branda et al. for allosteric inhibition [27], by Krämer et al. for allosteric regulation of catalytic activity [28] and Haberhauer et al. for opening and closing a chiral hinge [29]. Even more impressively the *syn-anti* conformational change at bipyridine was used to drive a chirality pendulum (see Fig. 10). Upon metal-ion addition ( $\text{Cu}^{2+}$ ,  $\text{Zn}^{2+}$ ) the arms of the pendulum did swing from one configuration to the other: in the metal-free state the chiral scaffold enforces *P*-configuration of the pendulum arms, while in presence of metal ions the *M*-configuration dominates [30].

Phenanthroline-based nanomechanical switches have been explored by Schmittel et al. over the past five years. Using concepts of self-sorting that are based on the HETPHEN strategy

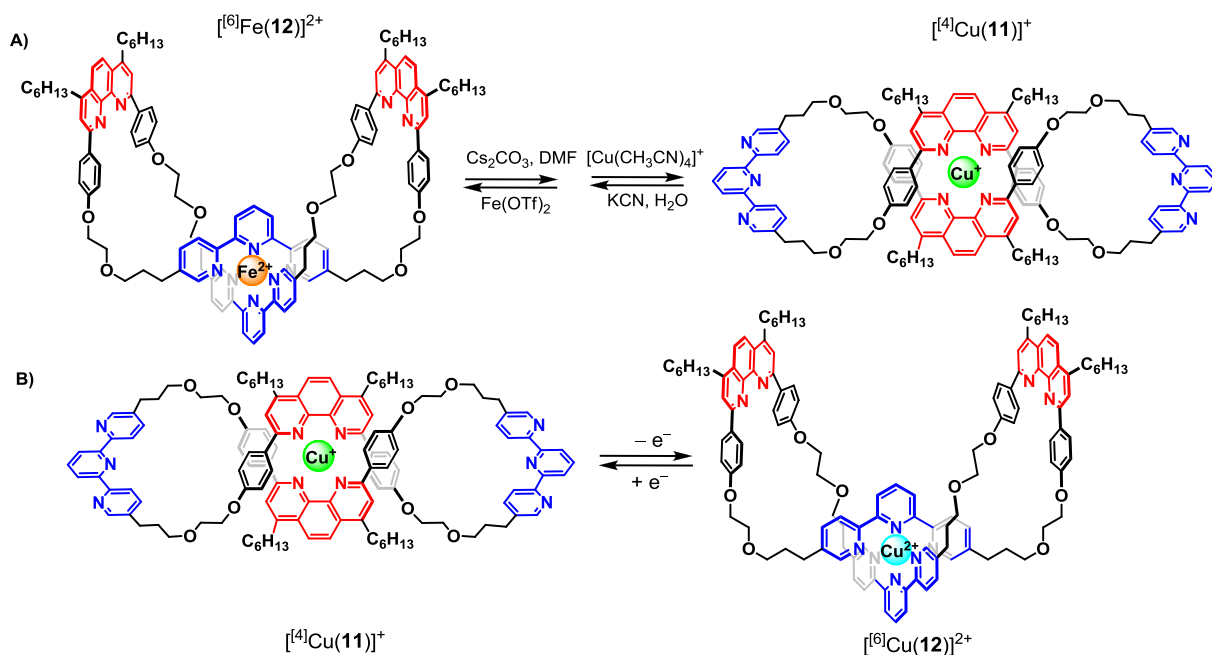


Fig. 8. Muscle-like dynamic systems: figure-of-eight complexes [18].

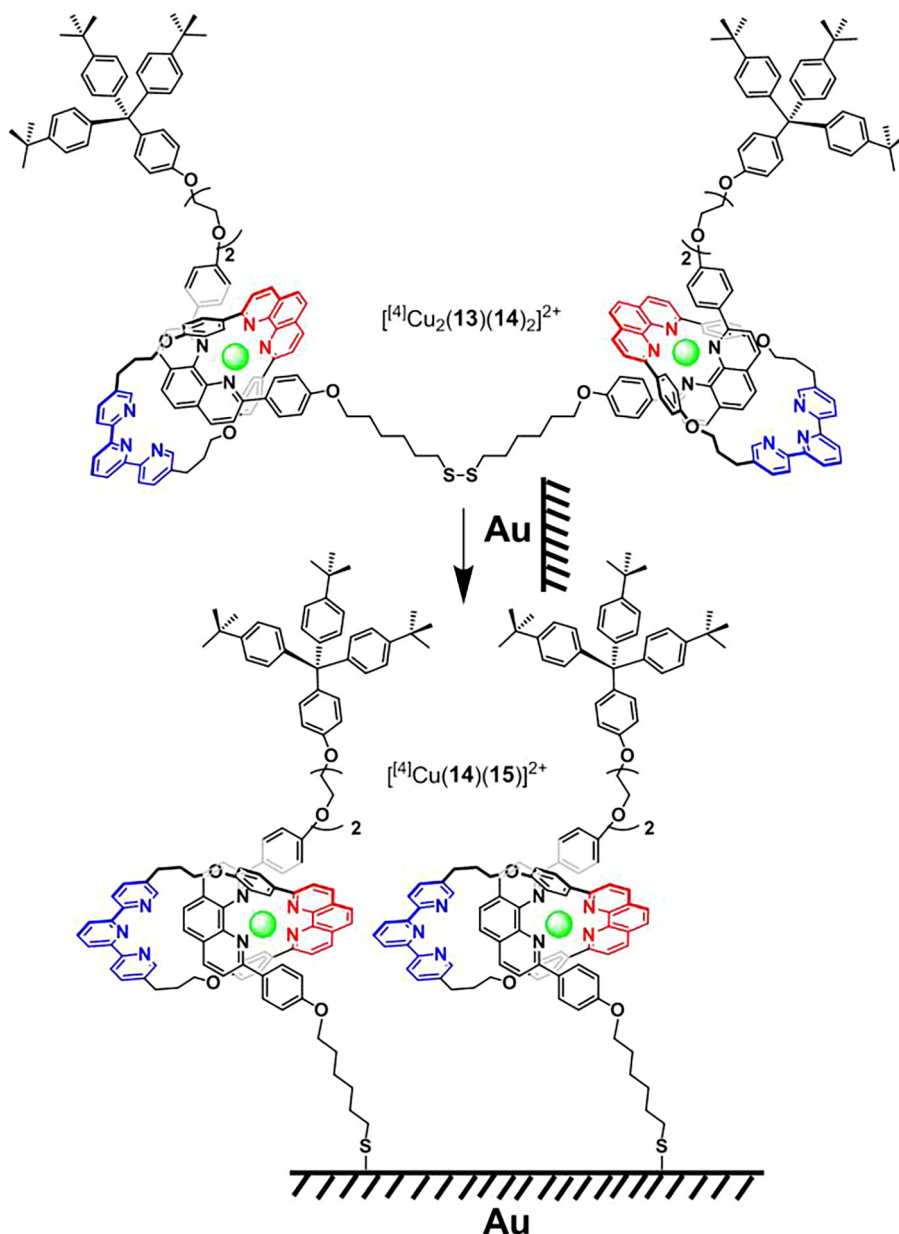


Fig. 9. Mounting rotaxanes on gold surface [21].

(HETeroleptic bisPHENanthroline metal complexation [31]) several nanoswitches with intramolecular heteroleptic bis(diimine) copper (I) complex sites were prepared for toggling via facile metal exchange [32], some of which are illustrated here. For opening of the diimine copper(I) coordinative bonds in  $[^{41}\text{Cu}(\mathbf{18})]^+$ , the nanoswitch was reacted with cyclam which entailed a toggling of the switching arm onto the zinc porphyrin (ZnPor) station. Incidentally, when irradiated at 419 nm, the copper complex is photochemically active transferring triplet energy to *cis*- $\mathbf{17}$  which readily isomerizes to *trans*- $\mathbf{17}$ , whereas  $\mathbf{18}$  (switching State I) is unable to support the photoisomerization (Fig. 11) [32]. Nanoswitch  $\mathbf{18}$  was also toggled via a redox protocol involving a redox-active phenanthroline [33].

Upon addition of copper(I) ions the hybrid terpyridine-phenanthroline ligand  $\mathbf{19}$  readily forms the intramolecular copper complex  $[\text{Cu}(\mathbf{19})]^+$  (State I in Fig. 12), a process that is easily reverted back to  $\mathbf{19}$  upon adding one equivalent of cyclam [34]. This cycle was repeated several times. Most importantly, though, when the closed copper(I) complex  $[\text{Cu}(\mathbf{19})]^+$  was reacted with

0.5 equiv. of  $\text{Fe}(\text{ClO}_4)_2$  the “dimeric” complex  $[\text{Fe}(\text{Cu})_2(\mathbf{19})_2]^{4+}$  (State II) was furnished. Details of this mechanism were not investigated, but it is clear that the driving force for the cleavage of the copper(I) complex arises from the strong iron(II) bisterpy complexation in State II. Addition of the strong iron(II) complexing agent, 4-*N,N*-dimethylamino-2,2':6',2''-terpyridine, regenerated State I.

In complex  $[\text{Fe}(\text{Cu})_2(\mathbf{19})_2]^{4+}$  the copper(I) ions in the shielded phenanthroline sites remain coordinatively unsaturated, a feature that was exploited for catalyzing the cyclopropanation of cyclooctene ( $\mathbf{20}$ ) with ethyl diazoacetate ( $\mathbf{21}$ ) [34]. When nanoswitch  $[\text{Cu}(\mathbf{19})]^+$  (= State I) was heated (55 °C for 4 h) together with the above reactants ( $[\text{Cu}(\mathbf{19})]^+$ ,  $\mathbf{20}$  and  $\mathbf{21}$  = 1:10:10), no transformation was detected (Fig. 12). After addition of 0.5 equiv. of  $\text{Fe}(\text{ClO}_4)_2$  (in relation to  $\mathbf{19}$ ) and heating (same conditions as above), the cyclopropanation toward product  $\mathbf{22}$  was successful (30% yield). Various control experiments ascertained that neither  $\mathbf{19}$ ,  $[\text{Cu}(\mathbf{19})]^+$  nor  $[\text{Fe}(\mathbf{19})_2]^{2+}$  are catalytically active under these conditions. This example is remotely reminiscent of the mode of action of the

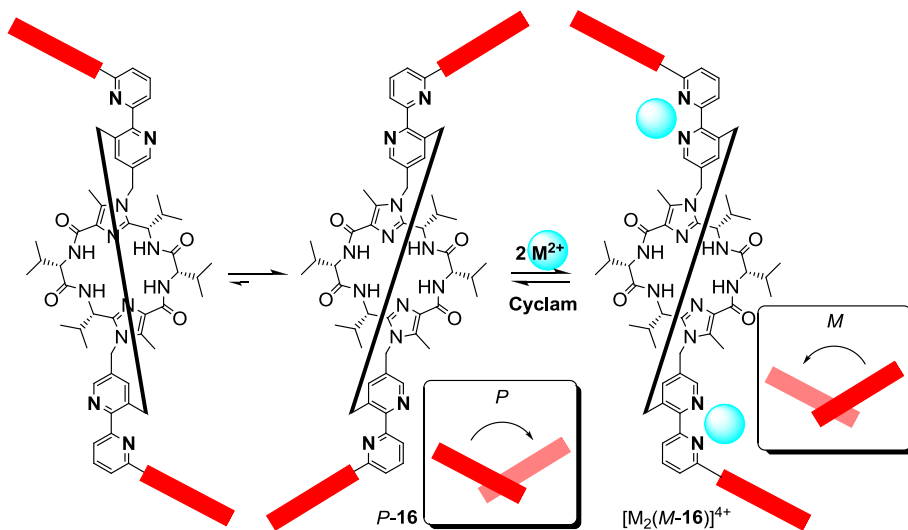


Fig. 10. A chirality pendulum activated by addition and removal of  $M^{2+}$  ions [30].

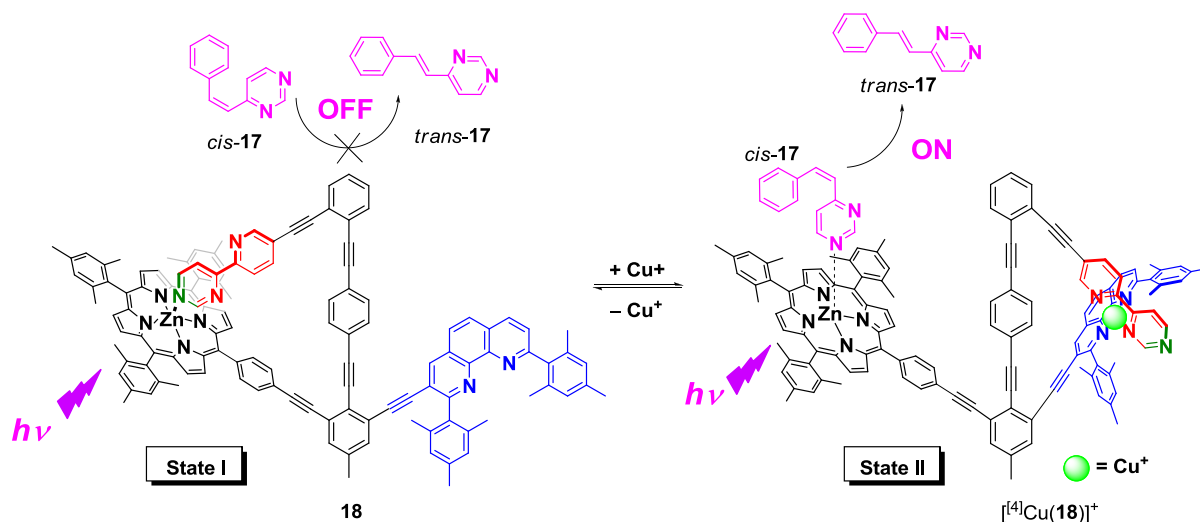


Fig. 11. Nanoswitch **18** acts as a triplet photosensitizer only in state II, i.e. as  $[^4Cu(18)]^+$  [32].

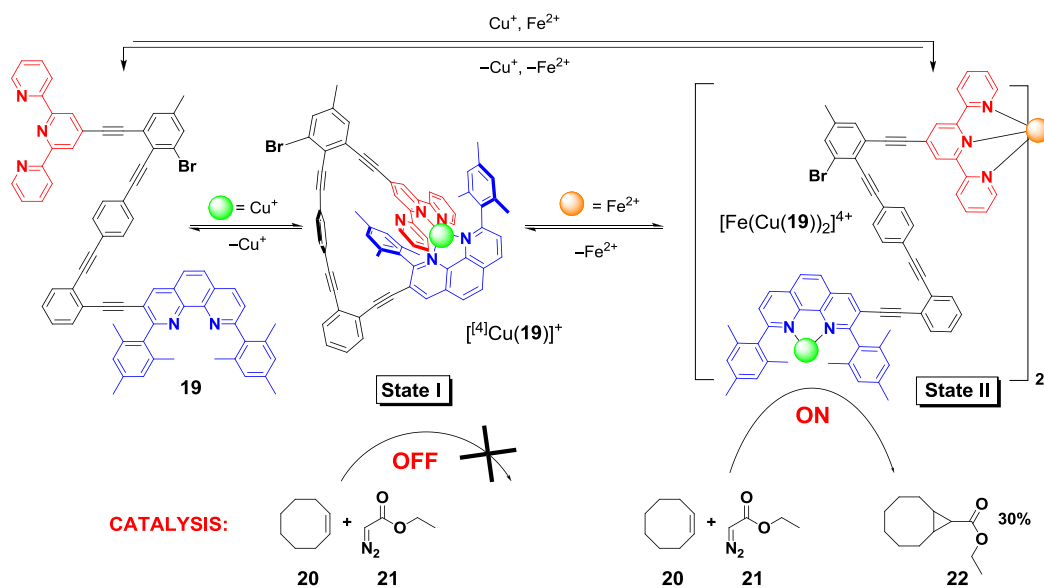


Fig. 12. Catalyzed cyclopropanation regulated by iron(II) via opening/closure of nanoswitch [34].



(SARS-CoV) 3C-like protease (3C<sub>1</sub>pro) [35]. In the monomeric state, the enzyme is inactive as its catalytic site is deeply buried in the collapsed state, whereas it is enzymatically active as a homodimer due to exposure of the active site.

A combination of intramolecular and intermolecular complexation reactions was used to enable nanoswitch **23** [36] to assume four distinct switching states (Fig. 13). As a prerequisite three orthogonal binding stations were implemented in **23** via zinc(II)-porphyrin (ZnPor), azaterpyridine and shielded phenanthroline binding sites. In state I, i.e. [Cu(**23**)]<sup>+</sup>, the copper(I) ion is buried between chelating phenanthroline and terpyridine ligand sites. Using a similar strategy as with [Cu(**19**)]<sup>+</sup>, addition of 0.5 equiv. of iron(II) ions to [Cu(**23**)]<sup>+</sup> cleaved the intramolecular copper complex and furnished the “dimeric” nanoswitch [Cu<sub>2</sub>Fe(**23**)<sub>2</sub>]<sup>4+</sup> in State II. After sequential removal of copper(I) and iron(II) ions state IV was reached which is characterized by the intramolecular N<sub>pym</sub> → ZnPor binding (pym = pyrimidine) (Fig. 13). The cycle was repeated several times without fatigue and used in a catalytic machinery to drive a catalytic process. This and other nanoswitches were used extensively by adding/removing copper(I) ions for toggling processes in controlling simple, dual [37] and even sequential [36] catalysis (*vide infra*).

Even five switching states were realized in nanoswitch **24** [38]. However contrary to the preceding switching protocol with four distinct inputs (Fig. 13), alternately copper(I) ions and the parent phenanthroline (**25**) were added with each addition toggling the switching arm from one site to another (Fig. 14). After addition of one equiv. of copper(I) ions to switch **24** the arm moved from

the ZnPor station to the newly copper(I)-filled phenanthroline site resulting in formation of complex [Cu(**24**)]<sup>+</sup> (although a terpyridine is involved, the copper is only tetracoordinated). Addition of one equiv. of **25** generated an intermolecular copper complex [Cu(**24**)(**25**)]<sup>+</sup> which causes the arm to shift back to the ZnPor site. The next two additions repeated the same toggling protocol at the second arm carrying a phenanthroline terminus. The toggling could be properly followed at the Q band of the zinc porphyrin unit (Fig. 15).

A fascinating machine based on a central, light-driven rotary motor and two oligobipyridine tails was designed by the Feringa group to switch between double-stranded metal helicates of distinct handedness [39]. In detail, once the *P,P* oligomer [Cu<sub>2n</sub>(**27**)<sub>n</sub>]<sup>n2+</sup> (with an intermolecular *P*-helicate) is irradiated, the motor turns into the *M,M* configuration with the copper(I) helicate maintaining the *P*-helicity. Since the *M,M*-configuration at the motor unit in *M, M, P*-[Cu<sub>2</sub>(**27**)]<sup>2+</sup> is thermodynamically disfavored, a thermal inversion to the *P,P*-motor unit is warranted which enforces a reorganization of the copper(I) helicate into *M'*-helicity. The inversion of the helicate (including motor inversion) takes place at a half-life of 327 days at 20 °C. The overall process was reversible (see Fig. 16).

While in the above example, the motor drives the reorganization at the metal complexation sites, in a converse approach, metal ion coordination influenced the speed of a motor [40]. Although reversible coordination of zinc(II) to a 4,5-diaza-9H-fluorene unit entails only tiny remote steric and electronic changes, Feringa et al. were able to allosterically regulate the speed of a light-driven motor.

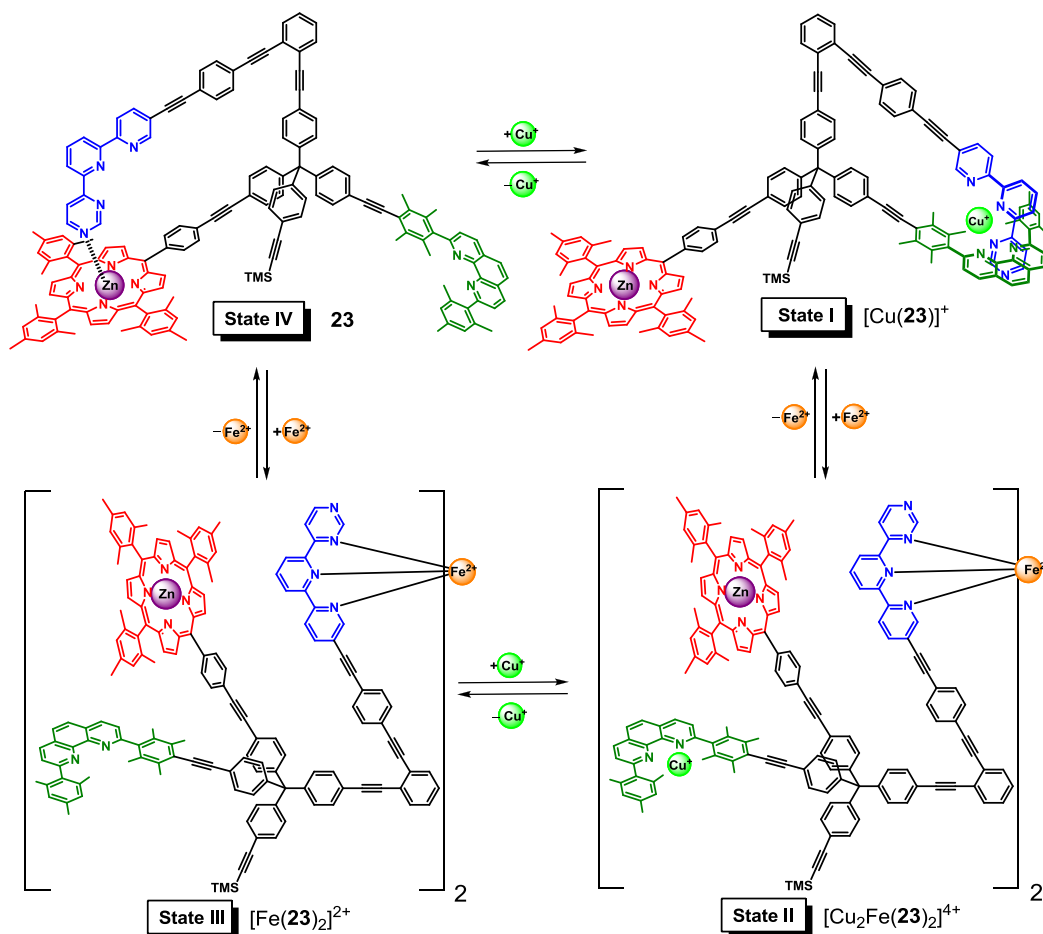


Fig. 13. Four-state switching in nanoswitch **23** [36].

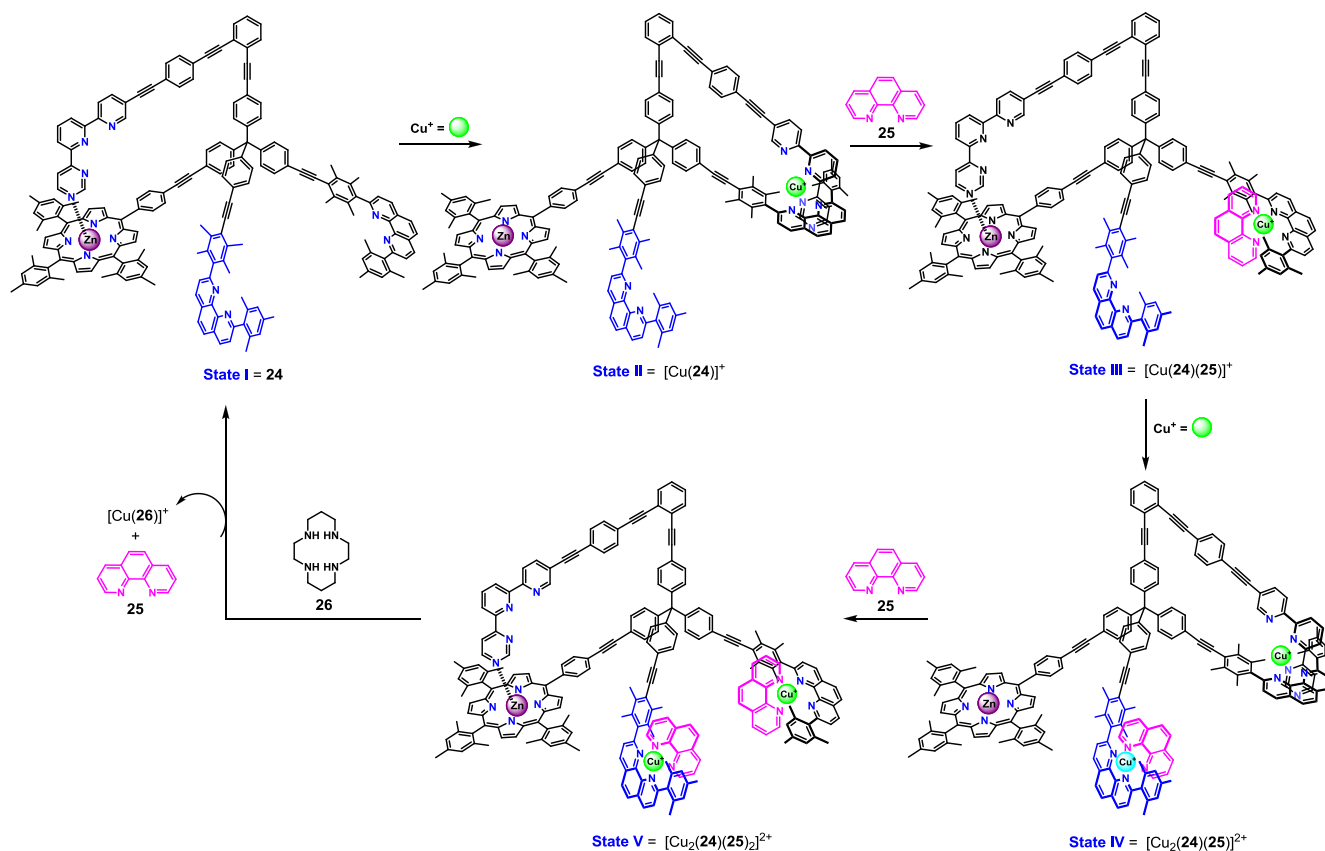


Fig. 14. Five-state switching in nanoswitch 24 [38].

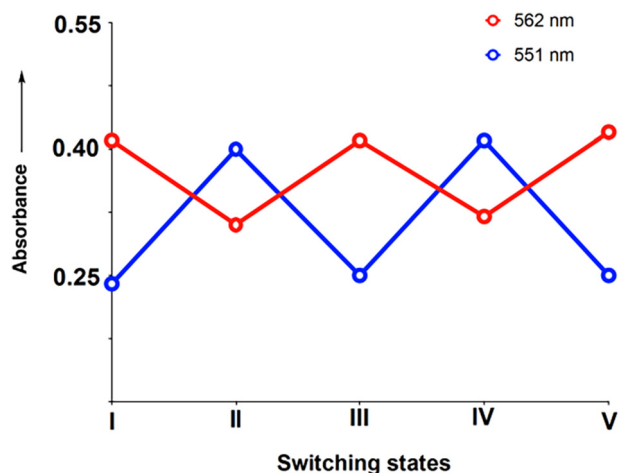


Fig. 15. Monitoring five-state switching at the Q band of nanoswitch 24 [38]. Reproduced from ref. [38] with permission of the American Chemical Society, copyright 2017.

### 2.3. Supramolecular switches, devices and machines

In this chapter we itemize some selected copper phenanthroline-based machines and switches. In these systems the constituents are neither topologically nor covalently linked. Due to the fact that such supramolecular aggregates can simply disintegrate by cleavage of coordinative bonds, their design and preparation have to take into consideration two additional factors: (i) The supramolecular aggregate has to form in a one-fold complete [41]

(integrative [42]) self-sorting, i.e. the formation of the supramolecular entity should be quantitative. (ii) Since the mode of action requires motion that itself is based on the cleavage of coordinative bonds, self-sorting has to be maintained during motion, i.e. self-sorting has to properly work not only in the spatial but also in the time domain. Considering that self-sorting is the key factor in design we have organized the present chapter along the number of components used in the corresponding devices, switches and machines. Such focus will not allow coverage of work that has been devoted to the (inter)conversion of supramolecular structures [43–47], for instance the supramolecular transformation depicted in Fig. 17 [44].

#### 2.3.1. Three-component machines

The HETPHEN strategy [31] has also found use in Nishihara's and Kume's three-component switches and rotors [48]. Their first example was based on the copper(I) 2,9-dianthracenylphenanthroline complex ( $[\text{Cu}(\mathbf{31})]^+$ ) as a stator using the 4-methyl-2-(2'-pyridyl)pyrimidine ( $\mathbf{32}$ ) as a rotator to obtain the heteroleptic complex  $[\text{Cu}(\mathbf{31})(\mathbf{32})]^+$  (Fig. 18). The *in/out*-interconversion (*io*) due to rotation at the pyrimidine ring was investigated at the copper(II)/(I) redox transition using cyclic voltammetry. At room temperature, two redox waves were observed in the cyclic voltammogram (CV) of  $[\text{Cu}(\mathbf{31})(\mathbf{32})]^+$ , reflecting the presence of both *io*-isomers. As copper(II) prefers a square-planar coordination in a tetracoordinate environment, the *i*-isomer  $[\text{Cu}(\mathbf{31})(\mathbf{32})]^+$  preferentially converts to the *o*-isomer  $[\text{Cu}(\mathbf{31})(\mathbf{32})]^+$  since there the methyl group is not interfering sterically (outer side) with the phenanthroline. Since ring rotation prompts a shift in the copper (II)/(I) redox potential, temperature-dependent switching (*i* → *o* inversion) was used to gate electron transfer events.

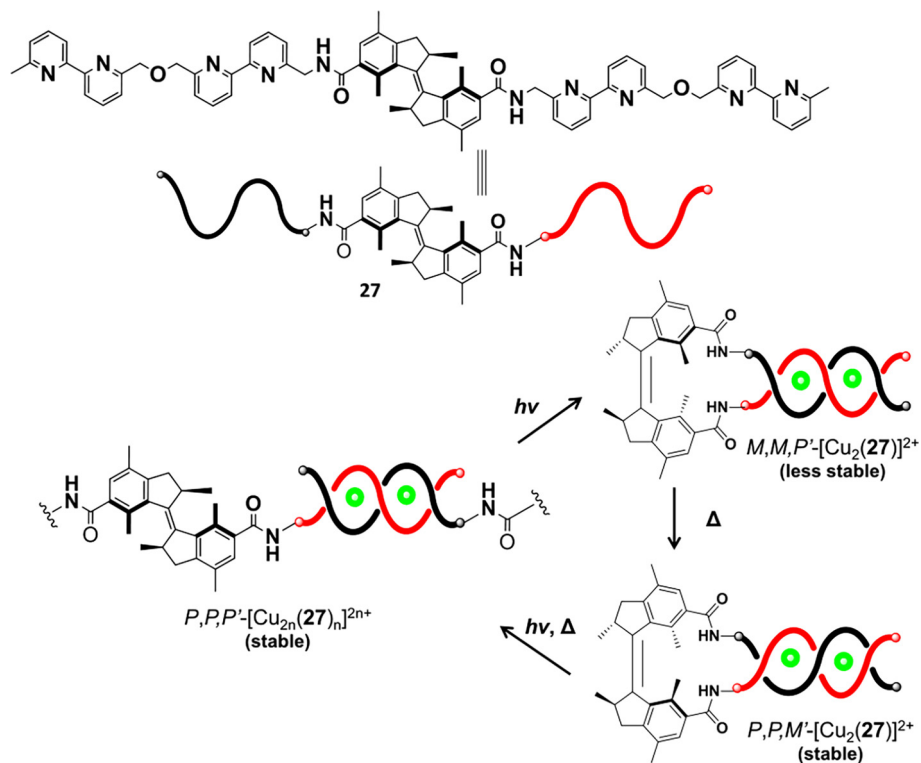


Fig. 16. Switching between double-stranded copper(I) helicates of distinct handedness [39].

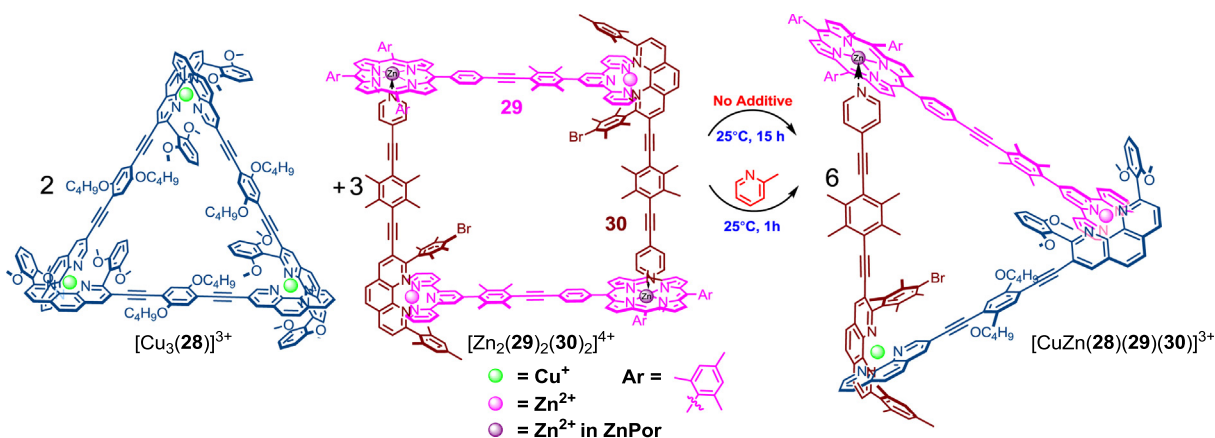


Fig. 17. Slow (without additive) and catalyzed fusion of two supramolecular structures to yield a scalene triangle [44].

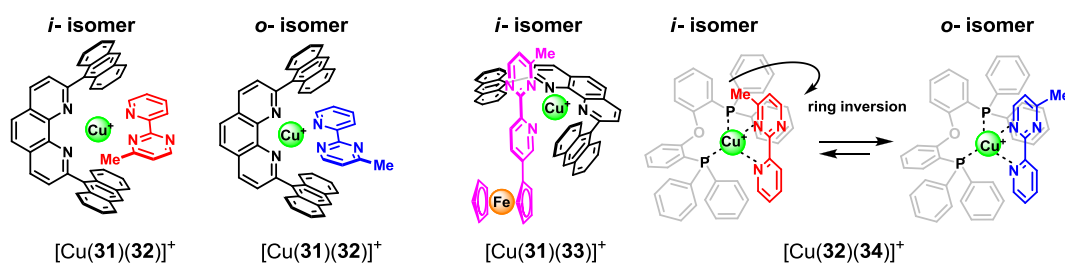


Fig. 18. Three-component switches operating via ring rotation.

Intramolecular electron gating was realized by attaching a ferrocene unit at the pyrimidine–pyridine ligand in  $[Cu(31)(33)]^+$  (Fig. 18) [49]. Due to the same reason as stated above, the *o*-isomer is highly favored after one- or two-electron oxidation.

the initial state, i.e.  $[Cu(31)(33)]^+$ , there is only a slight preference for the *i*-isomer ( $K_{i/o} = 0.44$ ). After one-electron oxidation, *o*- $[Cu(31)(33)]^{2+}$  is formed with the electron being removed from the copper center as indicated by the anisotropic EPR signal. As a

consequence of redox potentials, however, it is clear that initially the ferrocenyl group of the *i*-isomer is oxidized. After pyrimidine rotation the one-electron transfer redox potentials (copper(I)/(II) vs ferrocene/ferrocenium) are reversed triggering electron transfer from copper to ferrocene. For the three-component redox-active rotor, Kume and Nishihara optimized the rotational speed (inversion) by changing the steric preferences of the *i*-isomer using different groups adjacent to the pyrimidine nitrogen [50,51]. In combination with the diphosphine ligand **34** (Fig. 18), complex  $[\text{Cu}(\mathbf{32})(\mathbf{34})]^+$  exhibited mechanical bistability, which led to dual luminescence [52]. The inversion dynamics was found to depend on temperature and solvent. Rate constants for *i* → *o*-inversion were determined at 293 K in  $\text{CDCl}_3$  ( $k = 20 \text{ s}^{-1}$ ), acetone ( $k = 70 \text{ s}^{-1}$ ) and  $\text{CD}_3\text{CN}$  ( $k = 120 \text{ s}^{-1}$ ).

The thermal tristate rotor (twin rotor)  $[\text{Cu}(\mathbf{31})(\mathbf{35})]^+$  was established by same group capitalizing on the bipyrimidine ligand **35** as a rotator (Fig. 19) [53]. Since both pyrimidine rings are able to rotate with respect to the phenanthroline ligand, interconversion leads to three diastereomeric complexes (*ii* vs *io* vs *oo*). Thermodynamic and kinetic data of the full reaction coordinate were elucidated. The rate constants of interconversion reveal that the rates of *ii* → *io* (or *oo* → *io*) rotation are faster than those of the subse-

quent *io* → *oo* (or *io* → *ii*) rotation, leading to a relative stabilization of the *io* isomer.

So far, mechanical motion in redox-triggered machines had been based on the copper(II/I) redox couple, whereby a first-order rate behavior originated for the machine action in both directions. In contrast, Flood and his coworkers designed and executed a reversibly switchable copper(I) pseudorotaxane that operates on the reduction of the redox-active thread (Fig. 20) [54]. Quantitative formation of the [2]pseudorotaxane ( $[\text{Cu}(\mathbf{36})(\mathbf{37})]^+$ ) is guided by negative cooperative effects. Upon reduction of 3,6-bis(5-methyl-2-pyridine)-1,2,4,5-tetrazine (**37**) as the thread, an intermolecular self-sorting takes place furnishing the [3]pseudorotaxane  $[\text{Cu}_2(\mathbf{36})_2(\mathbf{37})]^+$ . This forward switching, which mechanistically involves electron transfer followed by supramolecular disproportionation ( $2 \times [\text{Cu}(\mathbf{36})(\mathbf{37})]^+ + e^- \rightarrow [\text{Cu}_2(\mathbf{36})_2(\mathbf{37})]^+ + \mathbf{37}$ ), follows a bimolecular associative interchange, as described in follow-up work [55]. The bimolecular reaction rate is sensitive to the denticity of the ligand ( $k_f(\mathbf{37}) = 12000 \text{ M}^{-1} \text{ s}^{-1}$ ), but not to electronic factors. In contrast, the reverse switching is a unimolecular dissociative process, which is consistent with a supramolecular de-threading-threading reaction ( $k_b = 50 \text{ s}^{-1}$ ). This detailed mechanistic investigation reveals an alternative switching modality to

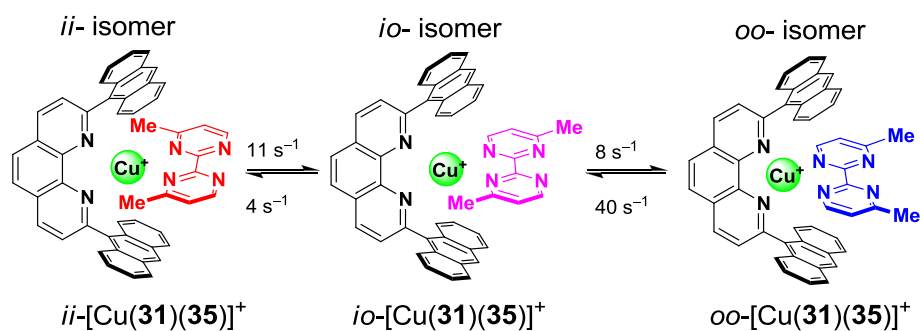


Fig. 19. Thermal tristate rotors [53].

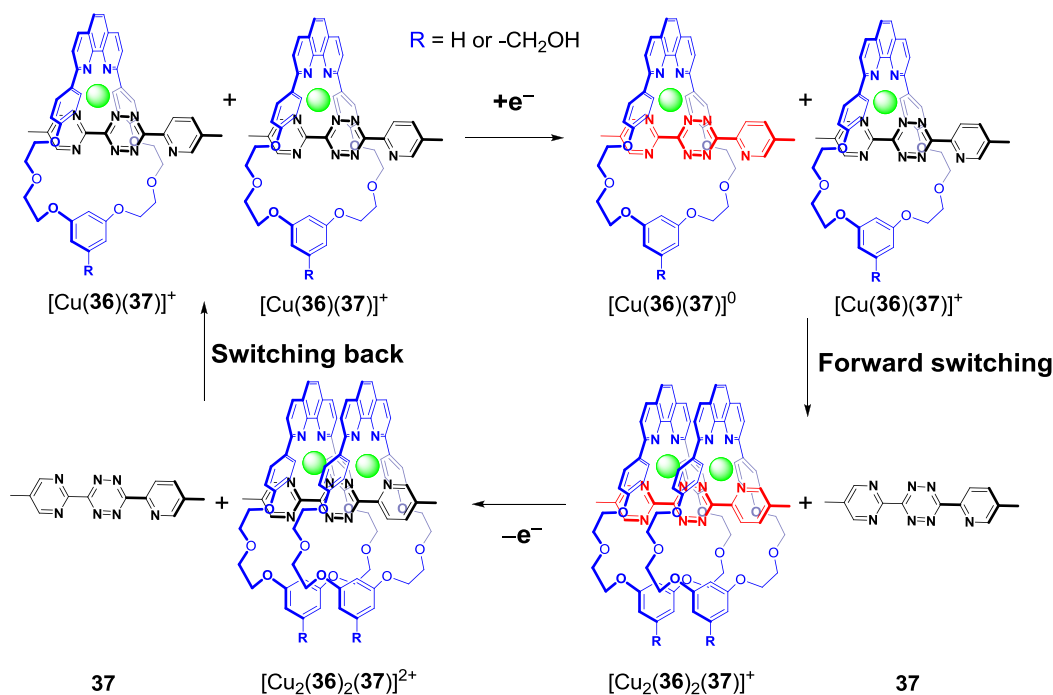


Fig. 20. Reversible switching of a copper(I)-based bistable [2]pseudorotaxanes into a [3]pseudorotaxane [54].

run molecular machines. A conceptually analogous approach was utilized by the same group for triggering a double switching protocol in palindromic [3]pseudorotaxanes [56].

The three-component device  $[^{41}\text{Cu}_2(\mathbf{25})_2(\mathbf{38})]^{2+}$  has been fabricated to allow for redox triggered cargo transfer from the phenanthroline to the pyridine-phenanthroline stations (Fig. 21) [57]. Upon loading the scaffold **38** with two copper(I) ions and two ligands **25**, the initial self-sorting generates the corresponding HETPHEN complexes on the phenanthroline stations of **38**. Upon oxidation, the self-sorting reshuffles ligands **25** toward the pyridine-phenanthroline stations. This process is reversible and can be investigated by cyclic voltammetry. Upon two-electron oxidation the self-sorted aggregate  $[^{41}\text{Cu}_2(\mathbf{25})_2(\mathbf{38})]^{4+}$  rearranges to  $[^{51}\text{Cu}_2(\mathbf{25})_2(\mathbf{38})]^{4+}$  at  $k = 10 \text{ s}^{-1}$  in  $\text{CH}_2\text{Cl}_2$ , whereas upon two-electron reduction the unstable  $[^{51}\text{Cu}_2(\mathbf{25})_2(\mathbf{38})]^{2+}$  undergoes reshuffling of the cargo at  $k = 5 \text{ s}^{-1}$  (at room temperature) finally affording  $[^{41}\text{Cu}_2(\mathbf{25})_2(\mathbf{38})]^{2+}$ .

### 2.3.2. Four-component switches and machines

The sterically shielded 2,9-diarylphenanthroline ligands ( $\text{phenAr}_2$ ) utilized in the HETPHEN concept [31] are by design unable to form bishomoleptic copper complexes due to high steric costs. Rather they exist in solution as  $[\text{Cu}(\text{phenAr}_2)(\text{S})_2]^+$  additionally coordinated by weakly binding solvent (S) molecules, in particular acetonitrile, which is present when one uses  $[\text{Cu}(\text{CH}_3\text{CN})_4]^+$  as copper source. As a result, any stronger binding monodentate ligand will replace the solvent molecule(s). For instance, pyridine (py) or pyrimidine (pym) ligands are readily bound to the coordinatively unsaturated  $[\text{Cu}(\text{phenAr}_2)]^+$  thus forming either  $[\text{Cu}(\text{phenAr}_2)(\text{py})]^+$ , i.e. so-called HETPYP-I complexes (HETeroleptic

Pyri(mi)dine/Phenanthroline), or  $[\text{Cu}(\text{phenAr}_2)(\text{py})_2]^+$  (HETPYP-II complexes) depending on the stoichiometry [58,59]. As a consequence of the rather weak binding, HETPYP complexes are highly dynamic and undergo a facile cleavage of the  $N_{\text{py}} \rightarrow [\text{Cu}(\text{phenAr}_2)]^+$  interaction upon heating. Based on this dynamic feature, Schmittel et al. have developed a variety of multicomponent nanorotors with rates between 0.1 and  $10^5 \text{ Hz}$  at room temperature. Most of the supramolecular nanorotors comprise four distinct components: (a) stator, (b) rotator, and two connectors, that is, (c) copper(I) and (d) a hinge (DABCO) as depicted in Fig. 22 [60]. The stator and rotator form a hetero-sandwich complex by means of two axial  $N_{\text{DABCO}} \rightarrow \text{ZnPor}$  bonds supported by two HETPYP-I interactions.

The intrasupramolecular exchange rate constant in the nanorotors based on cleavage of the dynamic  $N_{\text{py}} \rightarrow [\text{Cu}(\text{PhenAr}_2)]^+$  interaction has been measured and compared in various rotors with different stators and rotators, even in a five-component setup [61]. Rate measurements on five-component rotors with brake stones in their trajectory [62], however, do not allow conclusions to be drawn on the cleavage step. We thus focus our report on four-component rotors where the exchange rate has been varied by using rotators with one, two, or three pyridyl terminals [63]. By increasing the number of pyridyl terminals the activation energy for rotation increases and thus the rotational speed decreases as anticipated by thermodynamic considerations (Fig. 23). Remarkably it is not only the  $N_{\text{py}} \rightarrow [\text{Cu}(\text{PhenAr}_2)]^+$  coordinative bond, but also a good amount of dispersive attraction that has to be overcome in the rate-determining step. The dispersive attraction arises from interaction of the pyridine terminals and the large aryl substituents in the 2,9-positions of the phenanthroline stations. Furthermore, angular strain in rotors also plays a role

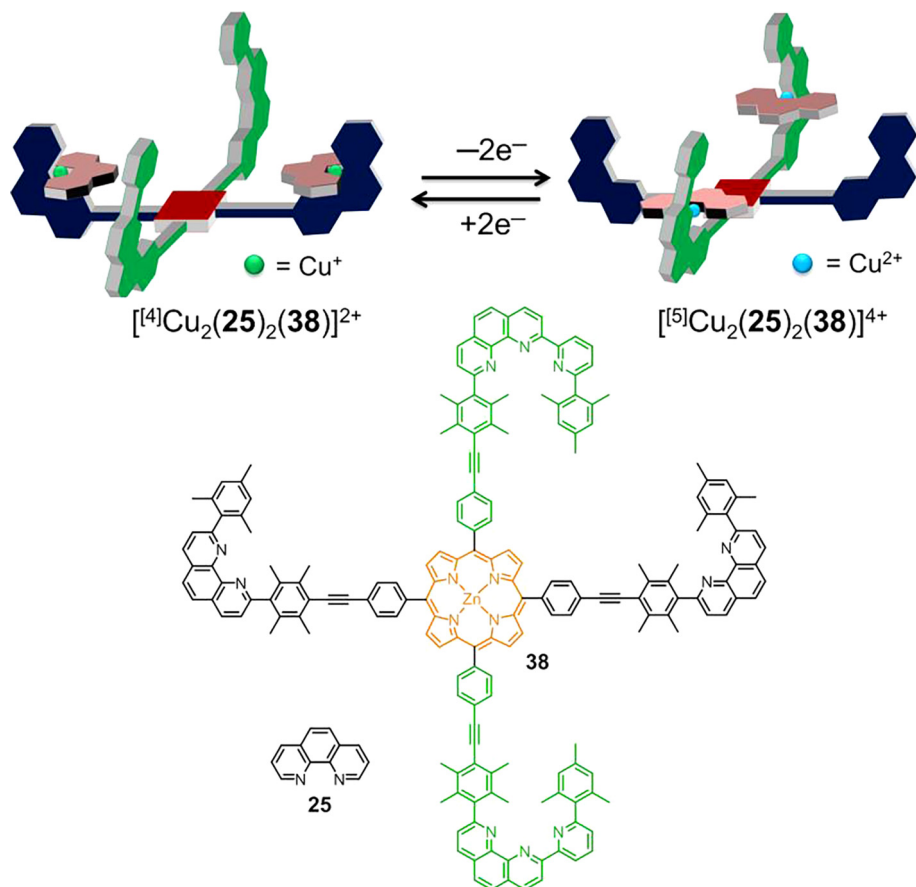


Fig. 21. Reshuffling cargo on a scaffold upon oxidation/reduction [57].



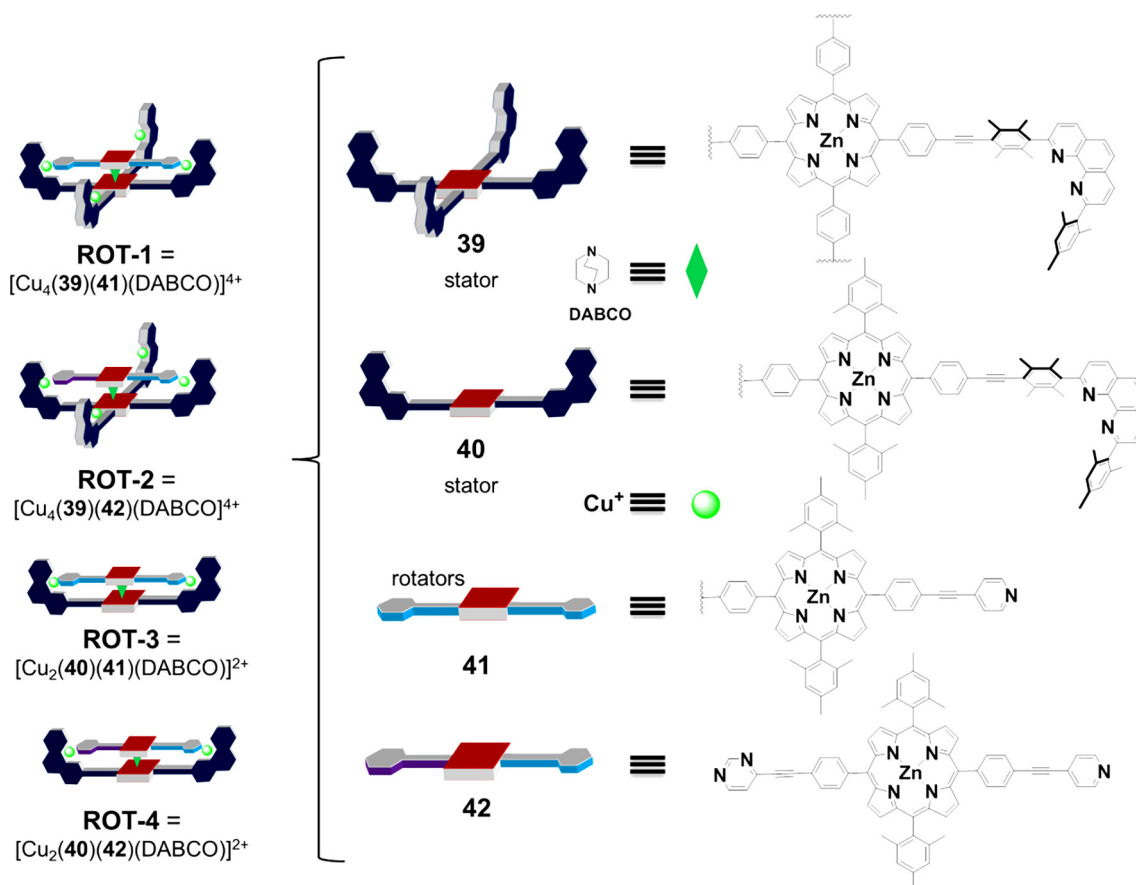


Fig. 22. Four-component nanorotors.

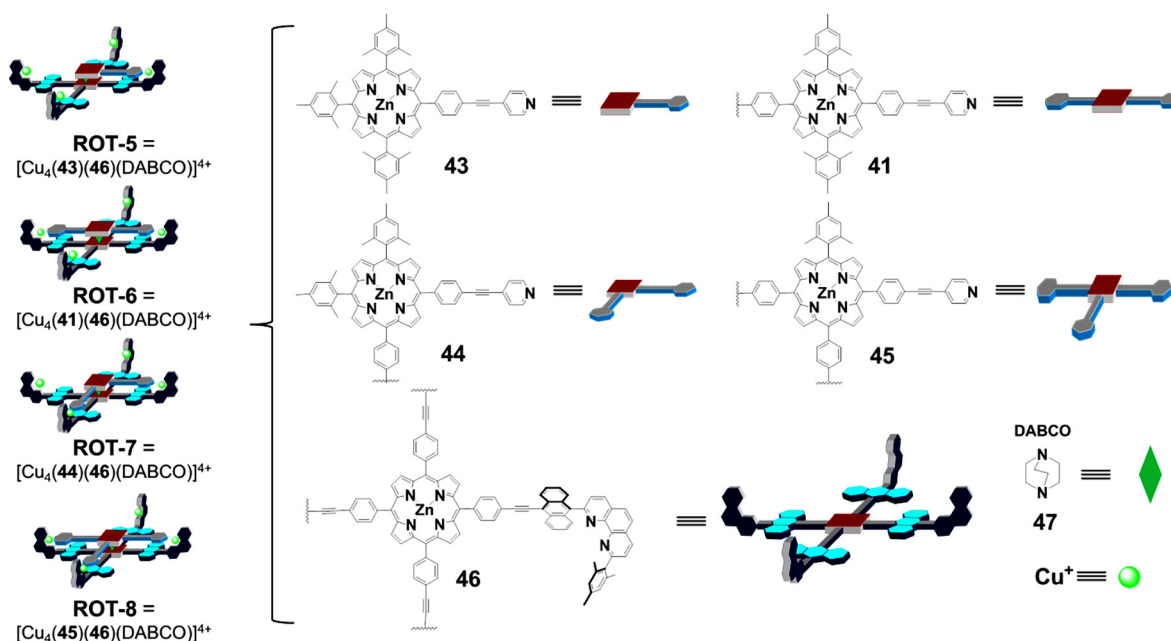


Fig. 23. Various other components in four-component nanorotors. Adapted from ref. [63] with permission of the American Chemical Society, copyright 2017.

as strain release in the departure step will lower the barrier. Considering the complexity of the rotational exchange process that is influenced by strain in the rotor, dispersive and coordinative inter-

actions, angular restrictions in the departure step and solvent interferences (*vide infra*) the quantitative assessment of all contributors to the dynamics is still limited.



### 3. Catalytic and networked multi-component machinery

#### 3.1. Self-sorting and multi-component machinery

In this chapter the very recent trend of multi-component machinery is highlighted. For a clear distinction, we identify “machinery” as a composite of at least two molecular devices or two entities with different functions that co-operate in a networked fashion thereby generating emergent function(s). Whereas self-sorting in stand-alone devices and machines can usually be solved with two or three orthogonal interactions, the design of machinery requires to handle orthogonality during various stages of communication and action so that a high level of command (= degree of self-sorting) is needed [41]. For a crisp description of machinery we will identify the number of (a) components and (b) functions. The number of components specifies all distinct molecular entities that have to be amalgamated to ascertain reversible operation of the machinery, while the “function” counts individual functional units whose action is synchronized.

#### 3.2. Catalytic machinery

**Double-function eight-component catalytic machinery:** The eight-component catalytic machinery in Fig. 24 is made up of eight distinct components, i.e. nanoswitch **48**, copper(I) ions, shielded phenanthroline **31**, piperidine (= catalyst, **49**), cyclam (**26**) and the reactants/product **50–52** of the catalyzed reaction [64]. The interaction of all components has to be harmonized when reversibly driving the machinery in the ON or OFF mode of catalysis. Looking from a different angle, the overall system links together two functional units, the nanoswitch and the catalyst. Nanoswitch **48** harbors three molecular subunits that are important for toggling: (1) a zinc porphyrin (ZnPor), (2) the pyrimidine nitrogen and (3) the bipyridine subunit within the azabipyridine switching arm. In  $\text{CH}_2\text{Cl}_2$ , nanoswitch **48** is locked with its arm on the ZnPor unit (state I). Toggling to State II is achieved by addition of copper(I) ions and 2,9-dianthrylphenanthroline (**31**) (1 equiv. each), because formation of the bulky intermolecular HETPHEN complex  $[\text{Cu}(\mathbf{31})(\mathbf{48})]^+$  at the bipyridine subunit is sterically incompatible with binding of the azabipyridine arm to the ZnPor unit.

In State II (Fig. 24), added piperidine will be strongly bound to the zinc porphyrin ( $\log K = 5.2$  [64]), while in State I it has to compete with the intramolecular azabipyridine arm for binding. Therefore, intermolecular attachment of piperidine in State I is rather weak ( $\log K = 2.4$ ). This binding difference can be used for ON/OFF switching of a catalyzed Knoevenagel reaction (conditions:  $55^\circ\text{C}$ , 30 min, in  $\text{CDCl}_3$ ). While in State II, piperidine is strongly bound and catalysis is prevented (OFF state of catalysis), the addition of one equiv. of cyclam (**26**) removes the copper(I) from

$[\text{Cu}(\mathbf{31})(\mathbf{48})(\mathbf{49})]^+$  generating the self-locked nanoswitch **48**. As a result, piperidine is released into solution, where it catalyzes the Knoevenagel reaction affording 23% of product **52**. The ON/OFF cycle was repeated three times without loss of activity [64]. In some ways, this switching protocol simulates the action of the calcium/calmodulin dependent protein kinase II (CaMKII) [65], the latter also being a self-locked system. To activate the enzyme, the inhibitory arm detaches from the active site after being wrapped up by a  $\text{Ca}^{2+}$ -loaded calmodulin.

**Triple-function ten-component catalytic machinery:** Three functions have to be molded in an interdependent fashion to enable toggling at nanoswitch **18** and the action of two catalysts, i.e. piperidine (**49**) and  $[\text{Cu}(\mathbf{53})]^+$  (Fig. 25) [37]. Full orthogonality of altogether ten components was required in the active mode of the catalytic machinery that is instructed to alternately command two catalytic processes. The reversible toggling of switch **18** (in States  $\text{I} \rightarrow 0 \rightarrow \text{II} \rightarrow \text{I}$ ) is a result of advanced self-sorting protocols which are based on the stoichiometric ratio of copper(I) ions and the constituents **18** and **53**. Importantly, the resulting three states exhibit alternate catalytic activity for two reactions.

A 2-fold complete self-sorting of **18**, **53** and  $\text{Cu}^+ = 1:1:2$  furnished the copper complexes  $[\text{Cu}(\mathbf{18})]^+$  and  $[\text{Cu}(\mathbf{53})]^+$  in a 1:1 ratio (State I). The change along States  $\text{I} \rightarrow 0 \rightarrow \text{II}$  was accomplished by addition of one equiv. of **53** for each switching step (Fig. 25), which thus involves self-sorting of **18**, **53** and  $\text{Cu}^+$  at ratios 1:2:2 and 1:3:2 affording  $[\text{Cu}(\mathbf{18})]^+ + [\text{Cu}(\mathbf{53})_2]^+$  (in State 0) and  $[\text{Cu}(\mathbf{18})(\mathbf{53})]^+ + [\text{Cu}(\mathbf{53})_2]^+$  (in State II), respectively. The cycle may be restarted from the beginning by addition of one equivalent of copper(I) ions to State II [37].

In State I complex  $[\text{Cu}(\mathbf{53})]^+$  is the catalyst for the click reaction of alkyne **54** and azide **55** affording product **56** (50%), whereas piperidine (**49**) is firmly bound to the zinc porphyrin unit of  $[\text{Cu}(\mathbf{18})]^+$  so that no catalysis of the Knoevenagel reaction is possible (Fig. 25). In State 0 the hitherto catalytically active  $[\text{Cu}(\mathbf{53})]^+$  is deactivated in the form of homoleptic complex  $[\text{Cu}(\mathbf{53})_2]^+$  while the piperidine remains inactive. Finally, in State II the switching arm is driven to the zinc porphyrin station of the nanoswitch where it liberates piperidine (**49**) into solution. Therefore piperidine is able to catalyze the Knoevenagel reaction generating 35% of product **52**.

**Triple-function eleven-component catalytic machinery:** Nanoswitch **23** and its various switching states have already been presented in Chapter 2.2. As in the preceding example, there are three functional items, i.e. nanoswitch **23** and two catalytic units, to be harmonized in their action. For switching and activating the catalytic units, nanoswitch **23**, copper(I) and iron(II) ions, piperidine (**49**) and two trapping reagents (cyclam (**26**) and 4-*N,N*-dimethylamino-2,2':6',2''-terpyridine (**57**)) need to cooperate smoothly. The switching as illustrated in Fig. 13 [36], is now executed in the

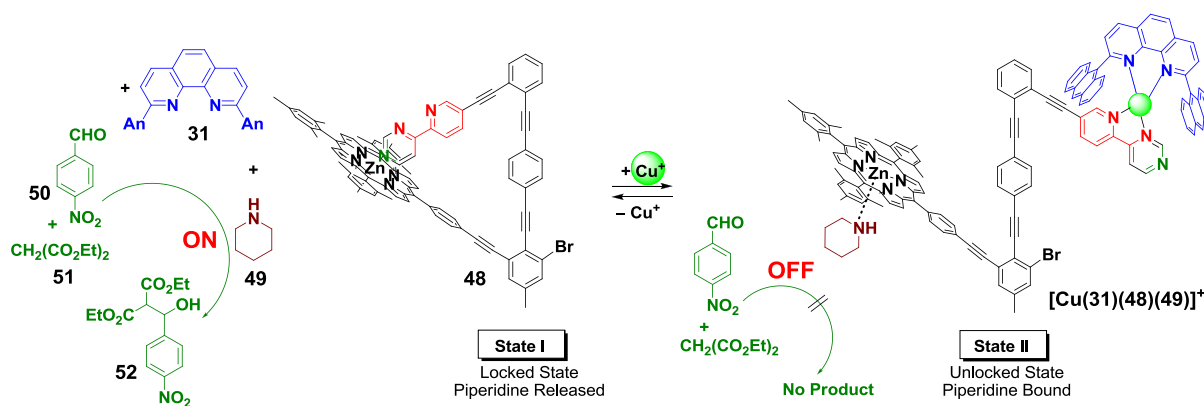


Fig. 24. Double-function eight-component catalytic machinery. Copper(I) ions are removed with cyclam (**26**) [64].

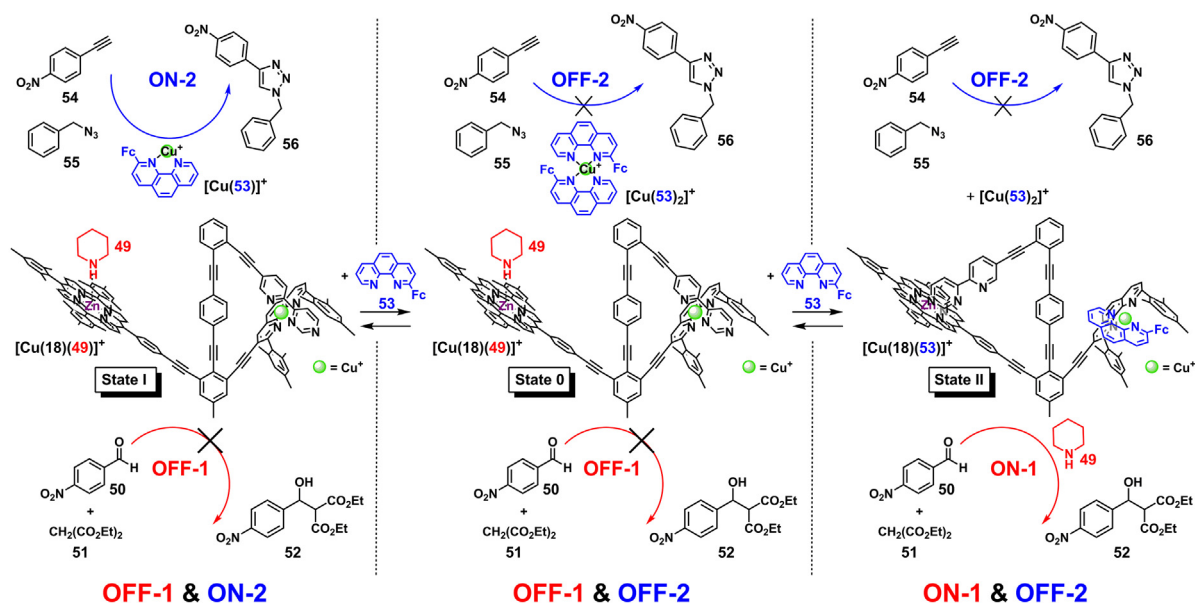


Fig. 25. Triple-function ten-component catalytic machinery alternately running two catalytic reactions [37].

presence of piperidine as a catalyst and the reactants **A**, **B** and **C** (Fig. 26). State I is catalytically inactive because the piperidine (**49**) is immobilized at the ZnPor unit of  $[\text{Cu}(\mathbf{23})]^+$  while the copper(I) ion in the heteroleptic complex is unavailable for catalysis. After addition of iron(II), State II is generated with the copper(I) ions exposed for catalysis. Indeed under the now chosen reaction conditions 50% of click product **AB** are formed. Removal of copper(I) ions leads to State III that is a resting state of catalysis. Removal of iron(II) furnishes nanoswitch **23** (= State IV). Now piperidine is released into solution so that click product **AB** undergoes a catalyzed follow-up Michael addition onto **C** to afford **ABC** in 28%. The second cycle fully reproduces the yields of the first run,

indicating that in total eleven components work together in an interference-free manner [36].

### 3.3. Networked catalytic machinery

The first examples of networked catalytic machinery have emerged in 2017. Different from the examples in Chapter 3.2, the external input toggles a nanoswitch which sends a second messenger to another switchable unit which itself is responsible for turning ON/OFF a catalytic process. As the two switchable systems have to work in an interdependent fashion we prefer the expression “NetStates” to describe the networked switching states.

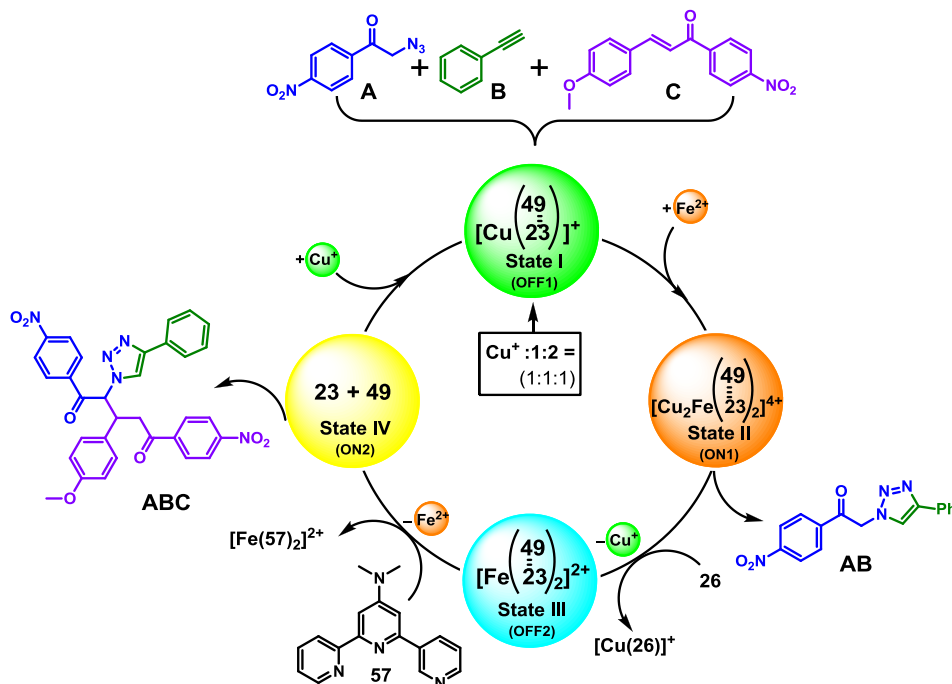


Fig. 26. Triple-function eleven-component catalytic machinery running two sequential catalytic processes (piperidine (**49**) is bound to the ZnPor unit of nanoswitch **23** in States I–III) [36]. For structures of switching states of **23**, see Fig. 13.

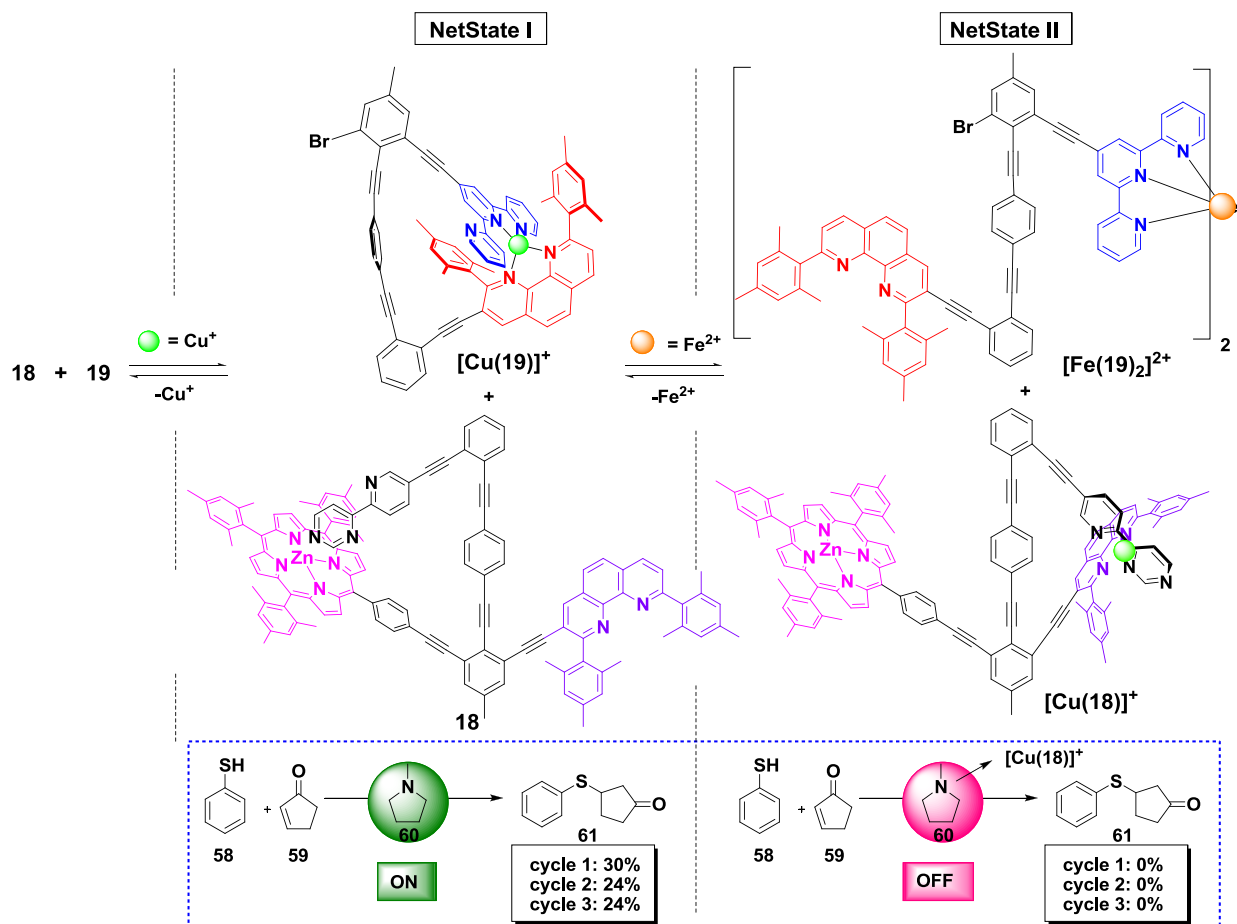


Fig. 27. Double-NetState nine-component catalytic machinery [66].

### 3.3.1. Double-NetState nine-component catalytic machinery

Formation of NetState I, represented by the 1:1 mixture of  $[\text{Cu}(19)]^+ + \mathbf{18}$  (Fig. 27), involves the superior self-sorting of  $\text{Cu}^+$  ion on nanoswitch **19** so that nanoswitch **18** remains devoid of copper(I) ion loading [66]. The follow-up transformation NetState I  $\rightarrow$  II embodies the communication step. It is effected by addition of  $\text{Fe}^{2+}$  ions to NetState I affording the dimeric iron(II) bisterpyridine complex  $[\text{Fe}(\text{Cu}(19))_2]^{2+}$ . In the latter dimeric complex the  $\text{Cu}^+$  ions are coordinatively unsaturated. They are only moderately bound to the shielded phenanthroline ( $\log K \approx 5.1$ ) of complex  $[\text{Fe}(\text{Cu}(19))_2]^{2+}$  and thus prefer to translocate into the HETPHEN coordination site of nanoswitch **18** ( $\log K \approx 8.1$ ). While this process is rapid at room temperature (3 min until completion), the reverse process (NetState II  $\rightarrow$  I) triggered by addition of the electron-rich 4-*N,N*-dimethylamino-2,2':6',2''-terpyridine (**57**) to afford  $[\text{Fe}(\mathbf{57})_2]^{2+}$  takes ca. 30 min as it involves the cleavage of the iron(II) bisterpyridine complex  $[\text{Fe}(\mathbf{19})_2]^{2+}$ .

The full catalytic machinery (Fig. 27) was tested in presence of reactants **58** and **59** [66]. In NetState I, *N*-methylpyrrolidine (**60**) is liberated as catalyst into solution where it catalyzes ( $\text{CH}_2\text{Cl}_2$ , 2 h,  $40^\circ\text{C}$ ) the conjugate addition of **58** onto **59** furnishing product **61** in 30% yield. Conversely, in NetState II, catalyst **60** is fully immobilized at the zinc porphyrin of  $[\text{Cu}(\mathbf{18})]^+$  so that no catalysis is detectable. The alteration of NetState I  $\rightarrow$  II  $\rightarrow$  I  $\rightarrow$  II  $\rightarrow$  I reproducibly furnished the catalytic ON (= NetState I) and OFF states (= NetState II), however, the yield of product **61** was consistently lower in the second and third cycle due to the slow switching of NetState II  $\rightarrow$  I.

Another double-NetState nine-component catalytic machinery now switched by redox inputs is displayed in Fig. 28 [67]. In Netstate I, the copper(I) ions are exclusively self-sorted on switch

**62** while upon one-electron oxidation of the ferrocenyl unit in **62**, a novel self-sorting reshuffles the copper(I) ions into the phenanthroline site of switch  $[\text{Cu}(\mathbf{23})]^+$  (NetState II). Reduction with decamethylferrocene (**64**) causes the copper(I) ions to translocate back, resetting NetState I. The translocations in forward (4 min at rt) and backward (1 min at rt) direction are rather fast. For catalytic action, NetState II is utilized to deactivate piperidine (**49**) at the ZnPor unit in  $[\text{Cu}(\mathbf{23})]^+$  ( $\log K = 5.37 \pm 0.41$ ) [36] whereas in NetState I piperidine is released into solution as it is only weakly bound to **23** ( $\log K = 2.66 \pm 0.08$ ). Indeed, in NetState I, the liberated catalyst **49** catalyzes the Knoevenagel addition between aldehyde **50** and diethylmalonate (**51**) generating product **52** in 26% yield in the first ON cycle, but only 20% in the second ON cycle. From various mechanistic investigations the conclusion was drawn that the oxidative conditions cause partial decomposition of the catalyst and thus reduce the yield in the second ON state [67].

### 3.3.2. Double-NetState nine-component machinery: rotation and catalysis

The next example highlights the ability of copper(I) not only to translocate in solution from one site to another but also to control self-assembly and disassembly of a catalytically active supramolecular nanorotor (Fig. 29) [68]. The self-sorting of copper(I) ions and ligands **62**, **65** & **66** furnishes  $[\text{Cu}(\mathbf{62})]^+$  and the pre-rotor assembly  $[(\mathbf{65})\cdot(\mathbf{66})]$  (= NetState I). Addition of zinc(II) ions displaces the copper(I) ions in the nanoswitch furnishing  $[\text{Zn}(\mathbf{62})]^{2+}$ , while the two equiv. of copper(I) ions are transmitted to the pre-rotor with concomitant formation of the nanorotor  $[\text{Cu}_2(\mathbf{65})(\mathbf{66})]^{2+}$  (= NetState II). Removal of zinc with hexacyclen regenerates NetState I.

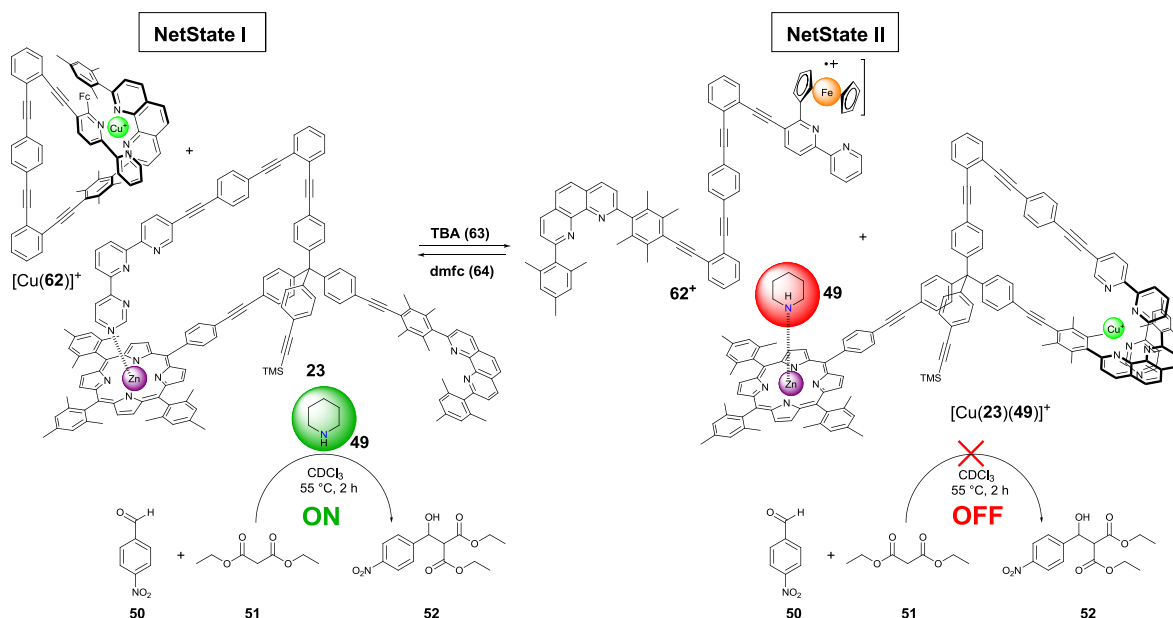


**Fig. 28.** Redox-triggered double-NetState nine-component catalytic machinery. **TBA** = tris(4-bromophenyl)aminium hexachloroantimonate; **dmfc** = decamethylferrocene [67].

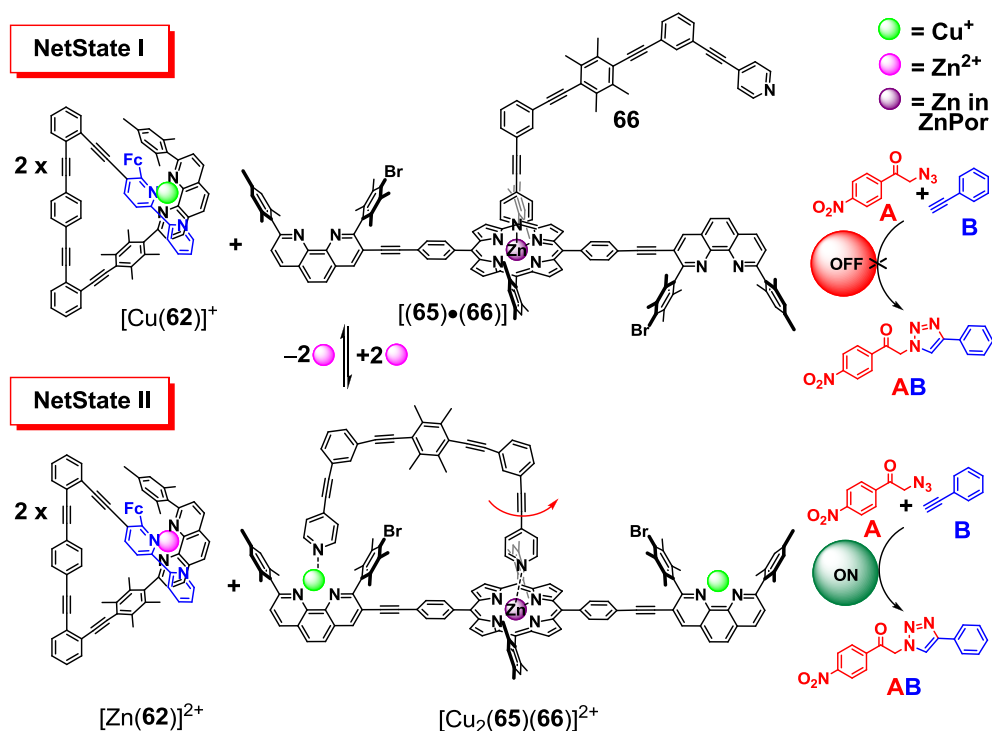


**Fig. 29.** Assembly and disassembly of catalytic rotary machinery [68].

The three-component nanorotor  $[\text{Cu}_2(\mathbf{65})(\mathbf{66})]^{2+}$  does not only rotate at high speed (46 kHz at room temp.) but is additionally active as a catalyst for the click reaction of **A** and **B** (Fig. 29). When NetState I was generated, no catalysis was detected. After addition of zinc(II) ions, however, the catalytically active nanorotor  $[\text{Cu}_2(\mathbf{65})(\mathbf{66})]^{2+}$  formed and catalyzed the formation of click product **AB**. The machinery was run through two ON/OFF cycles with identical yields of product **AB** (36%) in both rounds [68].

The examples in this chapter demonstrate impressively the extraordinary ability of copper(I) ions in combination with

phenanthroline binding sites to be highly dynamic and thus to be of great use in chemical signaling.

#### 4. Kinetic factors

##### 4.1. Kinetics in mononuclear copper(I) phenanthroline and diimine complexes

Despite the prevalence of copper(I) complexes in (supra)molecular devices there is remarkably little data with regard to their

kinetic behavior. If one uses the water exchange reaction at metal centers as a measure, copper(II) complexes experience extremely fast exchange rates with lifetimes approaching  $10^{-10}$  s [69]. Since copper(I) is not particularly stable in water, the corresponding numbers are missing in the water exchange investigation. Other fast exchanging metal complexes are those of  $\text{Cr}^{2+}$ ,  $\text{Cd}^{2+}$  and  $\text{Mn}^{2+}$ . Iron(II) complexes experience much slower exchange, but are still faster than those of iron(III) analogs. Notably, the measured rate constants of the most frequently used metal complexes cover almost 20 orders of magnitude [69] and suggest only few promising candidates for dynamic metal complex-based machinery (Fig. 30).

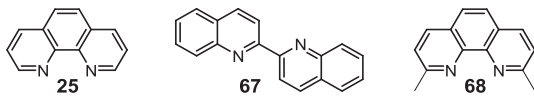
Exchange rates at transition metal ions depend on a variety of factors, including obviously the nature and charge of the metal, but also on steric and electronic effects of the ligand [70]. In addition, the ligand-field stabilization energy (LFSE) is considered to represent a barrier, because any dissociation or association breaks down the ligand field in the transition state. Contrastingly, Jahn-Teller distortion seems to support rapid exchange processes. These effects are particularly different for  $\text{Cr}^{3+}$  vs  $\text{Cr}^{2+}$  complexes (see Fig. 30).

Solvent assistance in inversion processes of copper(I) and silver(I) diimine complexes was already demonstrated in 1984 [71]. The most comprehensive kinetic studies on exchange reactions of copper(I) diimine complexes were performed by Geier in acetone, acetonitrile and solvent mixtures using direct methods [72]. A few relevant rate constants from this study are given in Table 1; they may serve as a crude lead. Accordingly, the ligand exchange reaction  $[\text{Cu}(\text{diimine})_2]^+ + \text{diimine}' \rightarrow [\text{Cu}(\text{diimine})(\text{diimine}')]^+ + \text{diimine}$  occurs at a bimolecular rate constant of ca.  $10^3 \text{ M}^{-1} \text{ s}^{-1}$  at 25 °C. Thus, at 1 mM of diimine' the lifetime of the exchange reaction would be as short as 1 s. Solvent assistance in diimine displacement reactions was confirmed with several nucleophilic solvents; the rate constant for exchanging 2,2'-biquinoline (67) by MeCN is  $1 \times 10^2 \text{ M}^{-1} \text{ s}^{-1}$  at 25 °C; in pure MeCN the lifetime is thus only 5 ms. Most remarkable is the accelerating effect of iodide that should allow catalysis of ligand exchange if used in substoichiometric amounts, a concept that has remarkably not been applied with molecular copper(I) complex-based machinery. Indeed, both steps, i.e. iodide association and dissociation are extremely fast reactions. Iodide used at a concentration of  $>3.2 \text{ mM}$  should outperform acetonitrile as solvent [72]!

Work by Thummel [73], who determined the kinetics of copper(I) complexes by VT NMR but unfortunately only at the coalescence temperature, demonstrates that – as expected – the exchange of a substituted phenanthroline ligand ( $\text{pK}_a = 4.8\text{--}5.5$  of parent 1,10-phenanthroline [74]) is slower than that of 2,2'-bipyrimidine ( $\text{pK}_a = 0.6$ ) due to weaker basicity. The activation barriers for both ligand systems are 48.5–58.5  $\text{kJ mol}^{-1}$  in acetonitrile. In agreement

Table 1

Rate and equilibrium constants of ligand-substitution reactions in acetone [72].



Ligand-substitution reaction	$k_{298}/\text{M}^{-1} \text{ s}^{-1}$	log $K$
$[\text{Cu}(\mathbf{68})_2]^+ + \mathbf{68} \rightarrow [\text{Cu}(\mathbf{68})_2]^+$	$4 \times 10^7$ (in MeCN)	7.0
$[\text{Cu}(\mathbf{67})_2]^+ + \mathbf{68} \rightarrow [\text{Cu}(\mathbf{67})(\mathbf{68})]^+ + \mathbf{67}$	$1.8 \times 10^3$	3.7
$[\text{Cu}(\mathbf{67})_2]^+ + \mathbf{25} \rightarrow [\text{Cu}(\mathbf{25})(\mathbf{67})]^+ + \mathbf{67}$	$3.8 \times 10^3$	2.2
$[\text{Cu}(\mathbf{67})_2]^+ + \text{MeCN} \rightarrow [\text{Cu}(\mathbf{67})(\text{MeCN})]^+ + \mathbf{67}$	$1 \times 10^2$	$\approx -4.4$
$[\text{Cu}(\mathbf{67})_2]^+ + \text{I}^- \rightarrow [\text{Cu}(\mathbf{67})(\text{I})]^+ + \mathbf{67}$	$6 \times 10^5$	$\approx 1.2$
$[\text{Cu}(\mathbf{67})(\text{I})]^+ + \mathbf{68} \rightarrow [\text{Cu}(\mathbf{67})(\mathbf{68})]^+ + \text{I}^-$	$2 \times 10^6$	$\approx 2.5$
$[\text{Cu}(\mathbf{67})(\text{MeCN})]^+ + \mathbf{25} \rightarrow [\text{Cu}(\mathbf{25})(\mathbf{67})]^+ + \text{MeCN}$	$\approx 1 \times 10^7$	

with solvent assistance, the coordinating solvent MeCN lowers the barrier in comparison to  $\text{CHCl}_3$  as solvent by ca. 5.0  $\text{kJ mol}^{-1}$ . Bulky substituents next to the coordinating nitrogen atoms lead to higher exchange barriers due to their interference in the solvent attack.

Because many diimine ligands, e.g. 2-substituted phenanthrolines and 6-substituted bipyridines, form chiral bis(diimine) copper(I) complexes, their configurational interconversion ( $P$  vs.  $M$ ) can be monitored in the presence of an enantiopure anion (Fig. 31). The resulting diastereomeric complexes have diastereotopic substituents and are thus easily differentiated in NMR experiments. The kinetic VT NMR evaluation of the configurational interconversion of diastereomeric salts by Sauvage [75,76] led to similar results as those by Thummel [73]: The exchange barrier of iminopyridines is lower than that of bipyridines which is again lower than that of phenanthrolines (Table 2). The lowest barrier was obtained for 6-*tert*-butylbipyridine (73) with  $\Delta G_{298}^\ddagger = 51.6 \text{ kJ mol}^{-1}$  ( $k_{298} = 5600 \text{ s}^{-1}$ ) as compared to that of 6-methylbipyridine (72) with  $\Delta G_{298}^\ddagger = 66.2 \text{ kJ mol}^{-1}$  ( $k_{298} = 16 \text{ s}^{-1}$ ). It is reasonable to assume that steric repulsion weakens the binding of the bipyridine nitrogen to the copper(I) center.

Using various chiral benzimidazole-pyridine ligands, the intramolecular  $\Delta/\Lambda$  isomerization ( $k = 0.3\text{--}4.3 \text{ s}^{-1}$ ) occurs at free activation energies  $\Delta G_{298}^\ddagger$  ranging from 66.7 to 71.4  $\text{kJ mol}^{-1}$  as measured by EXSY spectroscopy [77]. The barrier for the intermolecular exchange ( $\Delta G_{298}^\ddagger = 55.6\text{--}62.5 \text{ kJ mol}^{-1}$ ) is low but the bimolecular process obviously depends on the concentration of the added ligand ( $k = 70\text{--}1100 \text{ M}^{-1} \text{ s}^{-1}$ ). As the latter reactions show large negative activation entropies, an association mechanism is likely. Direct evidence for bimolecular adducts was established in related kinetic investigations [78]. In the same range, i.e. at 70  $\text{kJ mol}^{-1}$  (313 K) and thus at  $k_{313} = 14 \text{ s}^{-1}$ , the  $P$  ( $\Delta$ )  $\rightarrow$   $M$  ( $\Lambda$ ) interconversion of a copper(I) pyridine-imine complex was monitored in methanol [79].

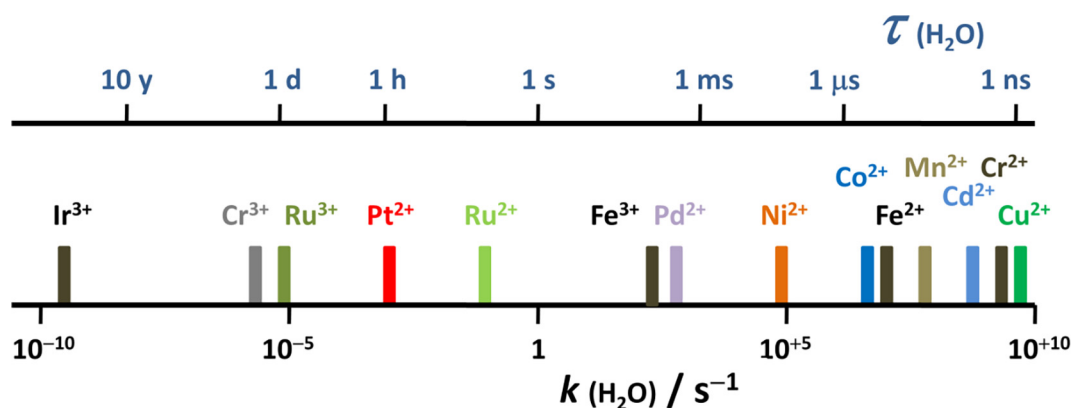


Fig. 30. Water exchange rates and lifetimes of metal complexes, adapted from [69].



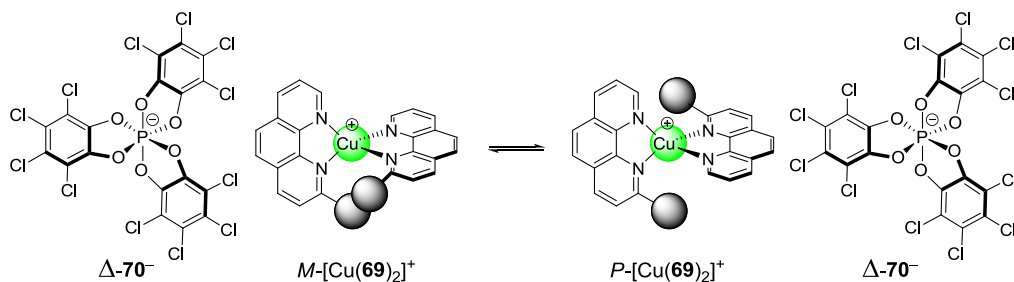


Fig. 31. Configurational interconversion of diastereomeric salts [75].

Table 2

Activation data of configurational interconversion in  $\text{CDCl}_3$  (cf. Fig. 31) [75].

Copper complex	$\Delta G_{298}^\ddagger / \text{kJ mol}^{-1}$	$k_{298} / \text{s}^{-1}$
$[\text{Cu}(\mathbf{71})_2]^+ + \Delta\text{-70}^-$	>68.0	<7
$[\text{Cu}(\mathbf{72})_2]^+ + \Delta\text{-70}^-$	66.2	16
$[\text{Cu}(\mathbf{73})_2]^+ + \Delta\text{-70}^-$	51.6	5600
$[\text{Cu}(\mathbf{74})_2]^+ + \Delta\text{-70}^-$	61.3	110

The dissociation kinetics of *bis*(2,9-dialkylphenanthroline)copper(I) complexes was measured within dimeric chiral helicates [80]. Whereas at 300 K and in  $d_2$ -TCE as a non-coordinating solvent the process was very slow ( $k_{300} = 6.3 \times 10^{-6} \text{ s}^{-1}$ ), it could be greatly accelerated by acetonitrile and upon heating. At higher temperature autocatalysis seems to play a role, possibly because racemization is then additionally driven by an  $\text{S}_{\text{N}}2$ -type process due to the presence of dissociated ligand. More detailed data about solvent effects was gained from ligand exchange studies at bis(imino-pyridine) copper(I) complexes in dicopper(I) helicates [81]: in acetone  $d_6$   $k = (1.6\text{--}1.8) \times 10^{-6} \text{ s}^{-1}$  ( $t_{1/2} = 110\text{--}120 \text{ h}$ ), in dichloromethane  $d_2$   $k = 4.9 \times 10^{-6} \text{ s}^{-1}$  ( $t_{1/2} = 40 \text{ h}$ ), and in acetonitrile  $d_3$   $k > 2 \times 10^{-3} \text{ s}^{-1}$  ( $t_{1/2} < 5 \text{ min}$ ) [82]. Thus acetonitrile leads to an acceleration of three orders of magnitude. As similar range was found for the inversion in a double-stranded helicate with ketimine-bridged tris(bipyridine) ligands [83]. The activation data in  $\text{CD}_2\text{Cl}_2$  were determined to  $\Delta H^\ddagger = 112 \text{ kJ mol}^{-1}$  and  $\Delta S^\ddagger = 22.1 \text{ J mol}^{-1} \text{ K}^{-1}$  along with  $k_{303} = 3.61 \times 10^{-6} \text{ s}^{-1}$  ( $t_{1/2} = 53.5 \text{ h}$ ).

Summarizing the heterogeneous kinetic data in Chapter 4.1 leads to the following insights: (1) ligand dissociation follows the expected trend of  $k$  (iminopyridine)  $>$   $k$  (bipyridine)  $>$   $k$  (phenanthroline); (2) steric and electronic effects at the ligand have a large influence, in particular if they are used to de-planarize chelating ligands, such as substituted bipyridines; (3) acetonitrile as solvent will easily speed up ligand exchange reaction by a factor of 1000 as compared to a non-nucleophilic solvent; (4) iodide may be used as a catalyst for ligand exchange reactions at copper(I) centers.

#### 4.2. Topologically controlled switches, devices and machines

The development of topologically controlled devices as already narrated using some selected examples in Chapter 2.1 has prompted Jean-Pierre Sauvage to undertake a variety of rate measurements in order to speed up the desired nanomechanical motions. The first example [6], published in 1994, exemplified how electrochemical input leads to a swing from a tetracoordinated bisphenanthroline copper(I) complex in [2]-catenate  $[\text{Cu}(\mathbf{1})]^+$  to the pentacoordinate phenanthroline terpyridine copper

(II) complex in catenate  $[\text{Cu}(\mathbf{2})]^{2+}$  (see Fig. 2). By EPR it was demonstrated that the oxidation of  $[\text{Cu}(\mathbf{1})]^+$  generates the copper(II) complex as a metastable species in a pseudo-tetrahedral configuration, i.e.  $[\text{Cu}(\mathbf{1})]^{2+}$ . Electrochemical and chemical oxidation allowed determination of the kinetics of the forward and backward process. The  $[\text{Cu}(\mathbf{1})]^{2+} \rightarrow [\text{Cu}(\mathbf{2})]^{2+}$  transformation in  $\text{CH}_3\text{CN}$  occurred at  $k_f = 2 \times 10^{-5} \text{ s}^{-1}$  ( $20^\circ\text{C}$ ;  $t_{1/2} = 9.6 \text{ h}$ ), while the reverse transformation  $[\text{Cu}(\mathbf{2})]^{2+} \rightarrow [\text{Cu}(\mathbf{1})]^+$  happened at  $k_b = 1 \text{ s}^{-1}$  ( $t_{1/2} = 0.7 \text{ s}$ ) [6]. The somewhat slower rate constants, by comparison with open copper(I) complex dissociation rate constants, were explained with topological constraints.

The above  $[\text{Cu}(\text{phen})_2]^{+/2+} \rightleftharpoons [\text{Cu}(\text{phen})(\text{terpy})]^{+/2+}$  reorganizations were later compared with analogous processes in rotaxanes, in which the macrocycle moves along the thread (= shuttle) [12] or the thread pirouettes from one site of the macrocycle to the other [13]. The case of a shuttle (Fig. 32), i.e.  $[\text{Cu}(\mathbf{5})]^+$ , was studied at  $25^\circ\text{C}$  in pure acetonitrile alike  $[\text{Cu}(\mathbf{1})]^+$ . The process of  $[\text{Cu}(\mathbf{5})]^{2+} \rightarrow [\text{Cu}(\mathbf{6})]^{2+}$  operates at  $k_{298} = 1.4 \times 10^{-4} \text{ s}^{-1}$ ; at a half-life of  $t_{1/2} = 1.4 \text{ h}$  the motion is a little bit faster than that in  $[\text{Cu}(\mathbf{1})]^{2+}$  [12]. The kinetics of the reverse reaction, i.e. the  $[\text{Cu}(\mathbf{6})]^+ \rightarrow [\text{Cu}(\mathbf{5})]^+$  reorganization, was not determined exactly, but it was approximated from the electrochemical data as  $10^{-4} \text{ s}^{-1} \leq k_{298} \leq 10^{-2} \text{ s}^{-1}$ . The pentacoordinated species  $[\text{Cu}(\mathbf{6})]^+$  thus has a minimum lifetime of 69 s (Fig. 32). This is a remarkable increase as compared to  $[\text{Cu}(\mathbf{2})]^{2+} \rightarrow [\text{Cu}(\mathbf{1})]^+$ . This difference was assigned by the authors to a reduced steric shielding about the metal center in the  $[\text{Cu}(\mathbf{5})]^{2+}$  rotaxane against external reagents than in the catenane, indicating that acetonitrile may play an important role in the rate determining metal-ligand bond dissociation. This shuttling between two different sites was much slower than then the degenerate exchange seen in one of Stoddart's catenane ( $k = 101 \text{ s}^{-1}$  at  $13.5^\circ\text{C}$ ) which required the dissociation of a cyclobis(paraquat-p-phenylene)/hydroquinone complex in the rate-determining step [84].

A rather similar reorganization was kinetically studied in rotaxane  $[\text{Cu}(\mathbf{3} \ \& \ \mathbf{4})]^{n+}$  in a comparable solvent mixture ( $\text{CH}_3\text{CN}/\text{CH}_2\text{Cl}_2 = 4:1$ ) (Fig. 33) [13]. Both the forward and backward processes were faster than in the system  $[\text{Cu}(\mathbf{1} \ \& \ \mathbf{2})]^{n+}$ . While the  $[\text{Cu}(\mathbf{4})]^+ \rightarrow [\text{Cu}(\mathbf{3})]^+$  reorganization ( $k_b = 17 \text{ s}^{-1}$ ;  $t_{1/2} = 0.04 \text{ s}$ ) was faster than in  $[\text{Cu}(\mathbf{5} \ \& \ \mathbf{6})]^{n+}$  by  $>1000$ , the  $[\text{Cu}(\mathbf{3})]^{2+} \rightarrow [\text{Cu}(\mathbf{4})]^{2+}$  motion was accelerated by a factor of ca. 40 ( $k_f = 0.007 \text{ s}^{-1}$ ,  $t_{1/2} = 99 \text{ s}$ ). As the rate determining steps in both forward and backward direction require metal-ligand dissociation, possibly aided by acetonitrile, and since the ligands are structurally rather close, steric features may be responsible for the differentiation.

To increase the rate of reorganization in analogous rotaxanes, Sauvage et al. replaced the diarylphenanthroline of the thread by a sterically unpretentious bipyridine site. Both the reduced steric bulk and the higher flexibility of the bipyridine unit should allow the acetonitrile to more easily attack the copper center thus igniting dissociation at the bipyridine. When the rotaxanes  $[\text{Cu}(\mathbf{75} \ \& \ \mathbf{76})]^{n+}$  were investigated (Fig. 34), both transformations were



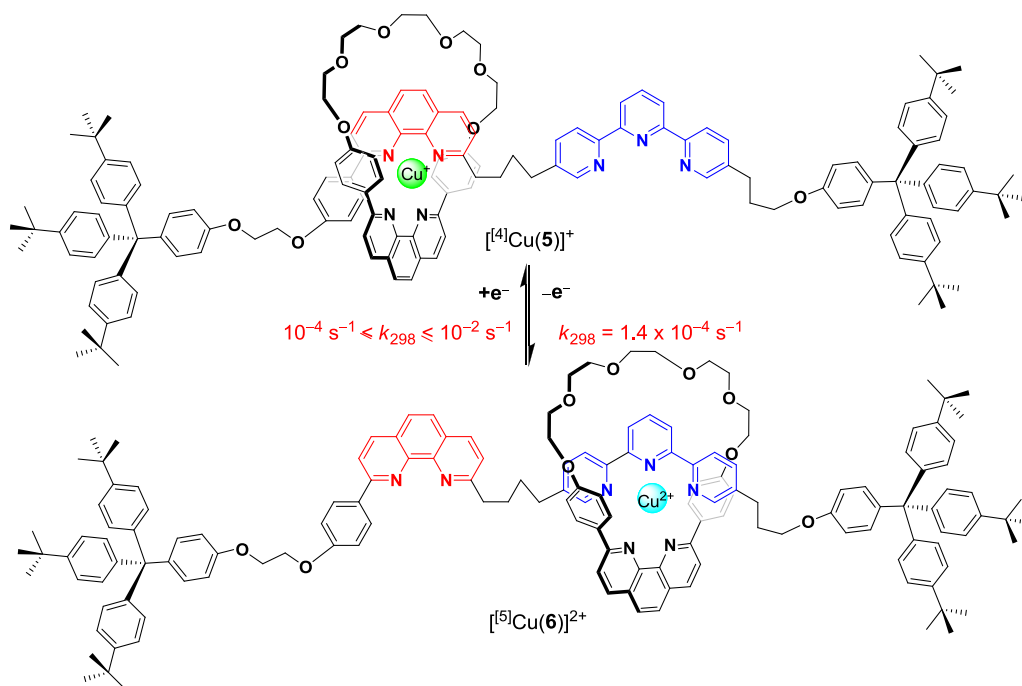


Fig. 32. A [2]rotaxane shuttle [12].

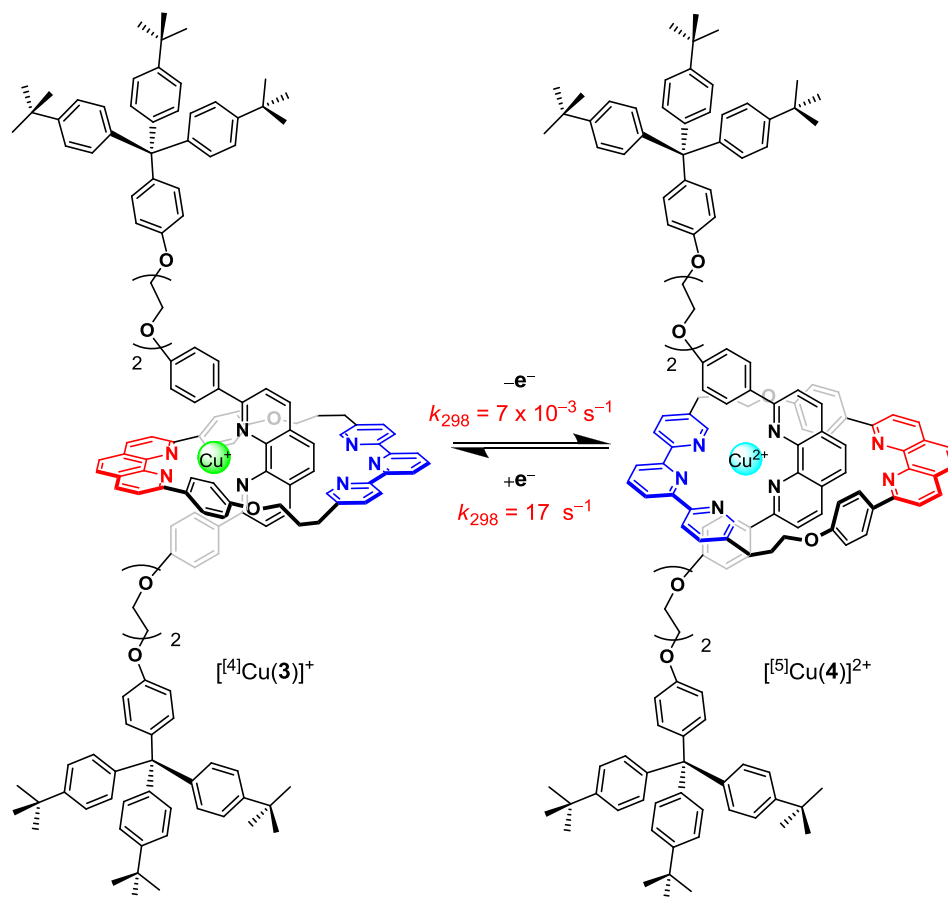


Fig. 33. A pirouetting [2]rotaxane [13].

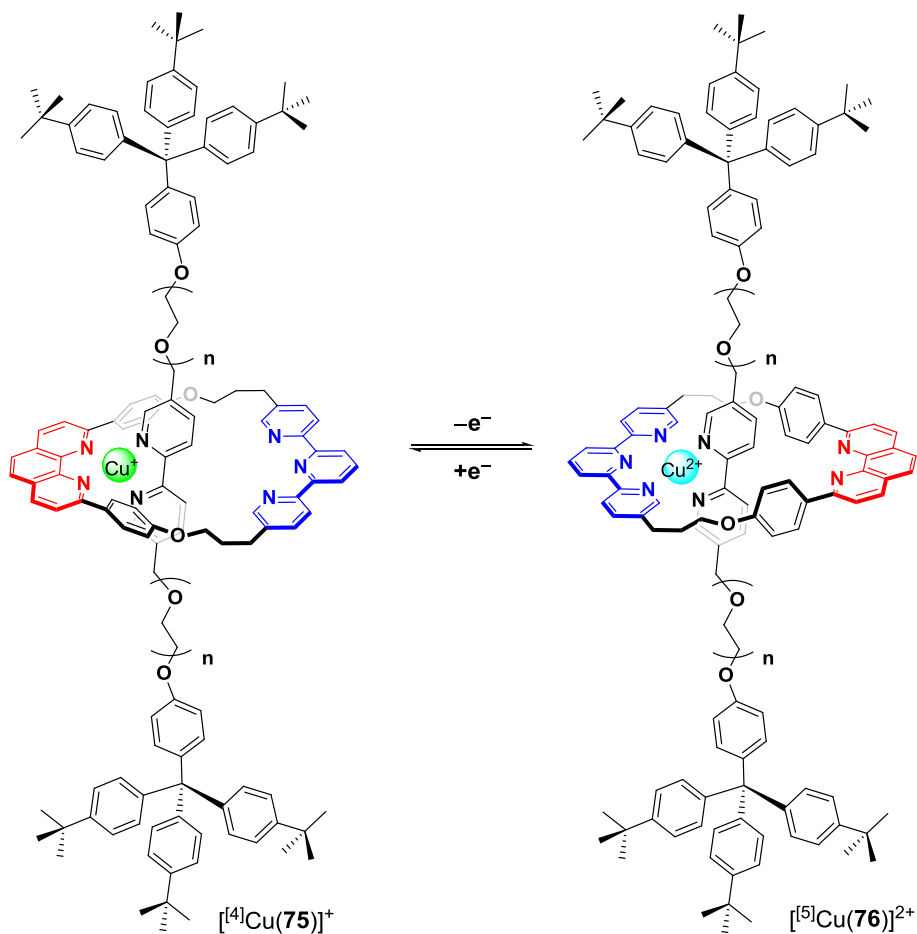


Fig. 34. A pirotaxane. Effect of the bipyridine unit in the thread [85].

indeed accelerated greatly (in  $\text{CH}_3\text{CN}$ ) as compared to  $[\text{Cu}(\mathbf{3} \ \& \ \mathbf{4})]^{n+}$ . The forward motion,  $[\text{Cu}(\mathbf{75})]^{2+} \rightarrow [\text{Cu}(\mathbf{76})]^{2+}$  ( $n = 1$ ), was accelerated by 600, the backward process, i.e.  $[\text{Cu}(\mathbf{76})]^{2+} \rightarrow [\text{Cu}(\mathbf{75})]^{2+}$ , by a factor of  $>29$ . A much faster system was surprisingly generated by spatially removing the stoppers from the copper complexation site ( $n = 3$ , in  $\text{CH}_3\text{CN}:\text{CH}_2\text{Cl}_2 = 9:1$ ) [85]. Even at  $-40^\circ\text{C}$  the system  $[\text{Cu}(\mathbf{75} \ \& \ \mathbf{76})]^{n+}$  ( $n = 3$ ) was faster by factor  $>2$  than the motion of  $[\text{Cu}(\mathbf{75} \ \& \ \mathbf{76})]^{n+}$  ( $n = 1$ ) at room temperature.

The analysis at this point demonstrates that the forward step  $[\text{Cu}(\text{phen})_2]^{2+} \rightarrow [\text{Cu}(\text{phen})(\text{terpy})]^{2+}$  is much more responsive

to steric shielding and conformational flexibility than the backward reaction  $[\text{Cu}(\text{phen})(\text{terpy})]^{2+} \rightarrow [\text{Cu}(\text{phen})_2]^{2+}$ . One possible reason is that in the backward reaction dissociation is more easily realized due to the inherent conformational flexibility in the terpyridine unit.

With these recipes at hand to accelerate the pirotaxing motion in rotaxanes, Sauvage further improved the shuttling motion in rotaxane  $[\text{Cu}(\mathbf{77} \ \& \ \mathbf{78})]^{n+}$  [86]. As a new coordination motif the 8,8'-diphenyl-3,3'-biisoquinoline subunit was implemented (Fig. 35), which is both conformationally flexible at the central

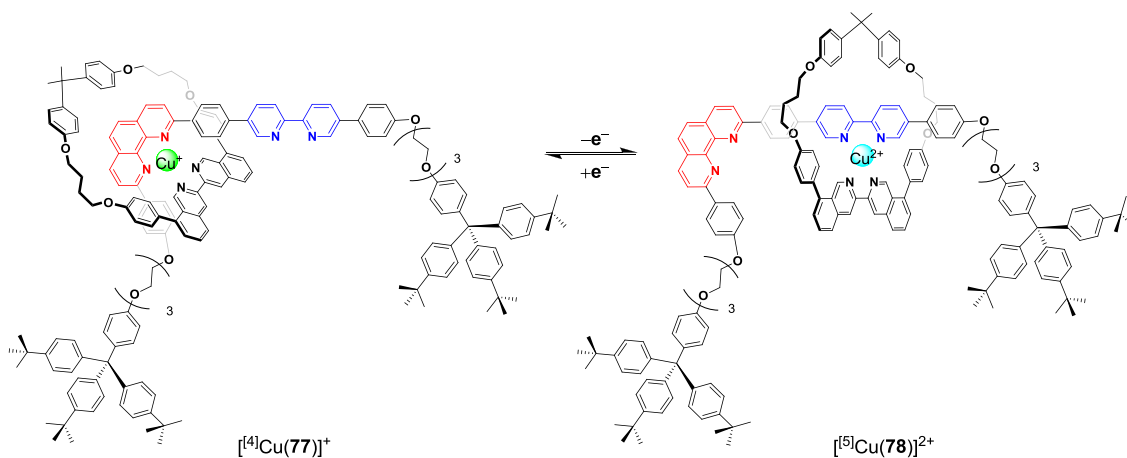


Fig. 35. A [2]rotaxane shuttle with improved shuttling rates [86].

diimine axis and less shielded due to the remote attachment of the macrocyclic linkage. Indeed, with regard to the former shuttle [Cu(5 & 6)]<sup>n+</sup>, this system underwent forward and backward shuttling (in MeCN/CH<sub>2</sub>Cl<sub>2</sub> (9:1)) more rapidly by a factor of 5700 and 5000 (see Fig. 35).

A further acceleration of the shuttling motion was achieved in rotaxane [Cu(79 & 80)]<sup>n+</sup> [87] by combining the 3,3'-biisoquinoline-based macrocycle with a sterically unencumbered alkyl chain at the phenanthroline (Fig. 36). In MeCN/CH<sub>2</sub>Cl<sub>2</sub> (9:1) this system underwent forward and backward shuttling more

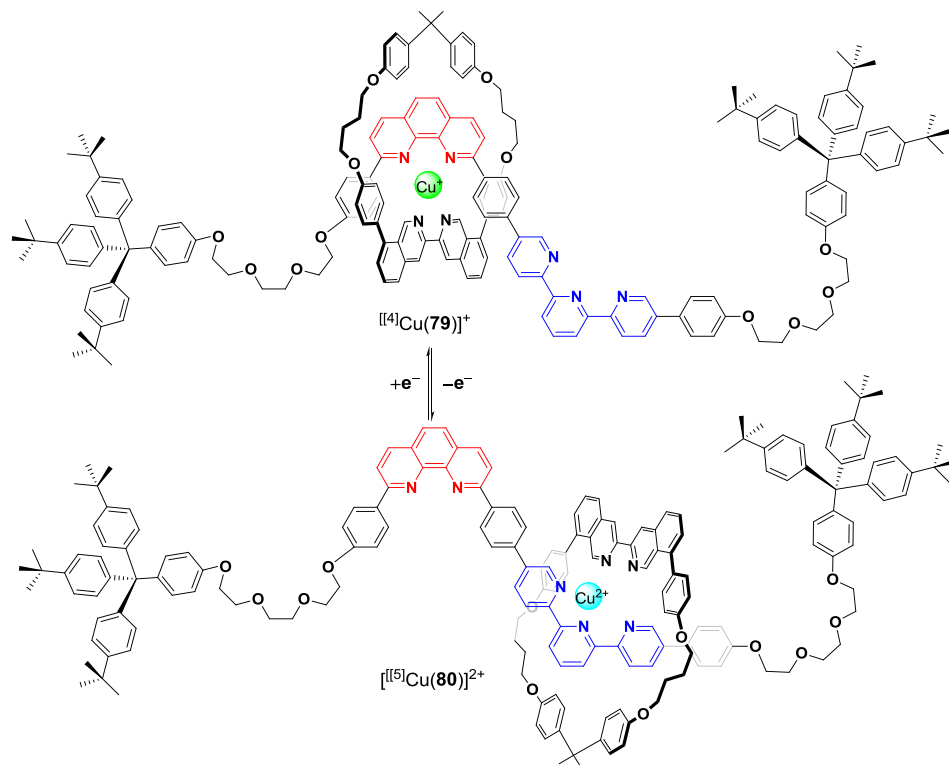


Fig. 36. A fast molecular shuttle [87].

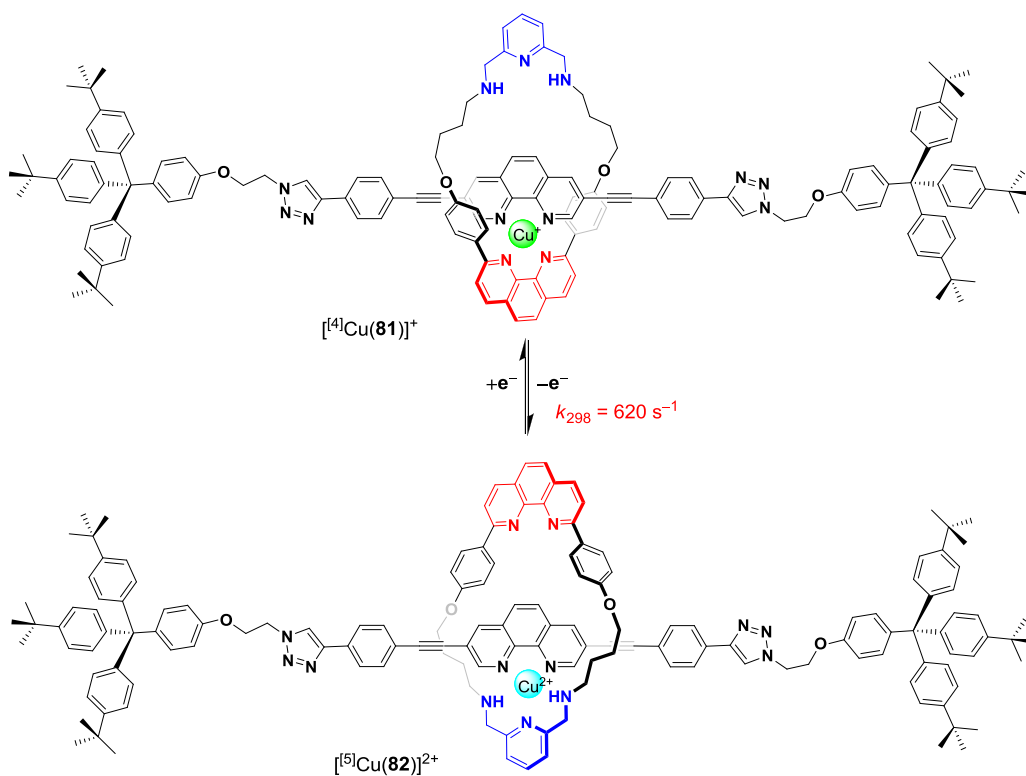


Fig. 37. The fastest shuttle reported up today [88].

rapidly than system  $[\text{Cu}(\mathbf{5} \ \& \ \mathbf{6})]^{n+}$  by a factor of  $10^4$  and  $>5000$ . In contrast, when a smaller and less flexible macrocycle was used, the species  $[\text{Cu}(\mathbf{1})]^{2+}$  was stable for several hours against rearrangement to  $[\text{Cu}(\mathbf{2})]^{2+}$  again suggesting a major influence of the migrating macrocycle on the overall rate.

Gavina and Tatay demonstrated that the rate constant for the pirouetting of rotaxane  $[\text{Cu}(\mathbf{81})]^{2+} \rightarrow [\text{Cu}(\mathbf{82})]^{2+}$  is as high as  $k_{298} = 620 \text{ s}^{-1}$  ( $t_{1/2} < 1.1 \text{ ms}$ ) in  $\text{CH}_2\text{Cl}_2$  (see Fig. 37) [88]. This rate constant is much higher than the fastest one of the Sauvage systems [89] although acetonitrile or other coordinating solvents were not used. It was argued that the unshielded phenanthroline in the thread is important for the high rate constant. This principle, somewhat modified, was used by the same authors to set up the fast shuttle  $[\text{Cu}(\mathbf{83})]^+$  (see Fig. 38) [90]. Using cyclic voltammetry the  $[\text{Cu}(\mathbf{83})]^+ \rightarrow [\text{Cu}(\mathbf{84})]^{2+}$  reorganization was determined as  $k_{298} = 2 \text{ s}^{-1}$  ( $\text{CH}_2\text{Cl}_2/\text{MeCN} = 1:9$ ). The solvent dependence was rather modest decreasing from  $k_{298} = 1 \text{ s}^{-1}$  at  $\text{CH}_2\text{Cl}_2/\text{MeCN} = 1:1$  to  $k_{298} = 0.6 \text{ s}^{-1}$  at  $\text{CH}_2\text{Cl}_2/\text{MeCN} = 9:1$  [90]. As the shuttling requires dissociation of the copper – phen<sub>macrocycle</sub> bond the acetonitrile seems to stabilize the copper (II) species in the gliding procedure.

In summary, the results by Sauvage and others on copper(I)-based shuttles and pirouettes demonstrate that the rate is increased if the available space about the copper center is opened up, in agreement with the rate determining step involving the dis-

placement of the coordinating ligands most likely aided by entering solvent. In the course of these structural improvements the rates could be accelerated by more than six orders of magnitude (see Table 3). Possibly even faster rates may arise if the rate-determining step only comprises cleavage of a pyridine → copper bond [91].

#### 4.3. Nanomechanical switches

Copper(I) ion is a premier choice for metal translocation studies [92], because its participation in cell signaling pathways has been convincingly demonstrated [93,94]. Direct kinetic information on copper translocation between two nanoswitches was gained from inverting the self-sorting preference after redox activation [95]. Upon treatment with one equiv. of copper(I) ions, the 1:1 mixture of **18** and **85** (see Fig. 39) ended up as a 97:3 ensemble of  $[\text{Cu}(\mathbf{18})]^+$  and  $[\text{Cu}(\mathbf{85})]^+$ . Upon addition of a one-electron oxidant, the resultant copper(II) ions self-sorted anew generating a 1:99 mixture of  $[\text{Cu}(\mathbf{18})]^{2+}$  and  $[\text{Cu}(\mathbf{85})]^{2+}$ , the latter stabilizing the copper(II) ions in a pentacoordinated environment (state II). Unfortunately, attempts to follow the kinetics of  $\text{Cu}^{2+}$  translocation were unsuccessful. Alternatively, the reaction  $[\text{Zn}(\mathbf{18})]^{2+} + \mathbf{85} \rightarrow \mathbf{18} + [\text{Zn}(\mathbf{85})]^{2+}$  was followed kinetically ( $25^\circ\text{C}$ ,  $k_{298} = 4.3 \times 10^{-3} \text{ s}^{-1}$ ,  $t_{1/2} = 161 \text{ s}$ ). Since metal translocation was zero order in the con-

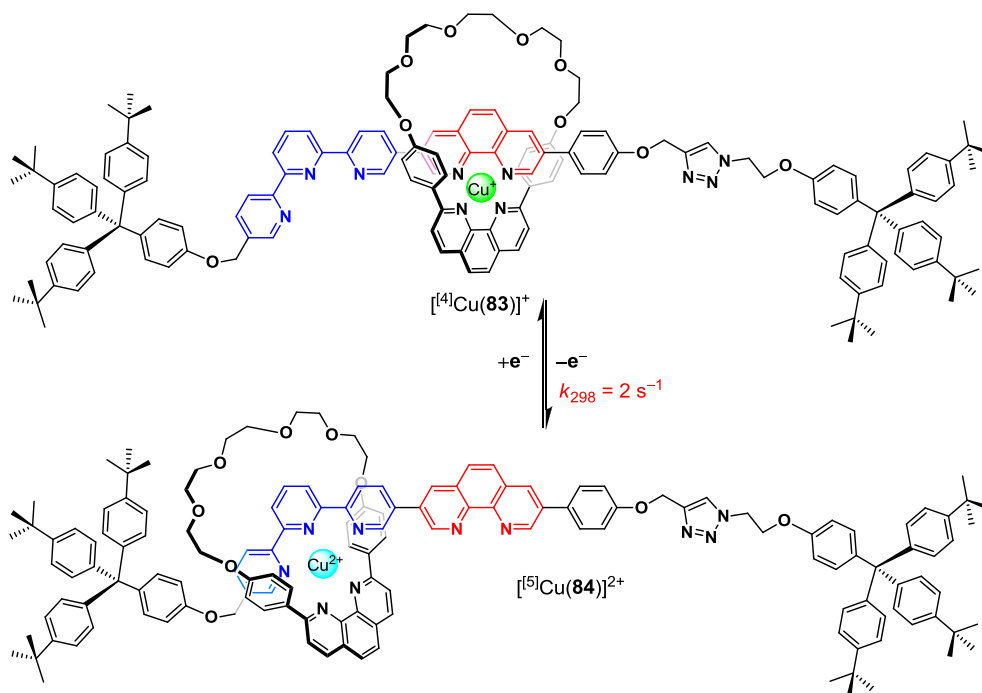


Fig. 38. A rapid shuttle [90].

Table 3  
Comparison of rate data from various machines.

	$[\text{Cu}(\mathbf{83})]^+ \rightarrow [\text{Cu}(\mathbf{84})]^{2+}$	$[\text{Cu}(\mathbf{85})]^+ \rightarrow [\text{Cu}(\mathbf{84})]^+$
$[\text{Cu}(\mathbf{1} \ \& \ \mathbf{2})]^+$ (shuttle)	$k_{298} = 2 \times 10^{-5} \text{ s}^{-1}$ ( $20^\circ\text{C}$ ; $t_{1/2} = 9.6 \text{ h}$ )	$k_{298} = 1 \text{ s}^{-1}$ ( $t_{1/2} = 0.7 \text{ s}$ )
$[\text{Cu}(\mathbf{5} \ \& \ \mathbf{6})]^+$ (shuttle)	$k_{298} = 1.4 \times 10^{-4} \text{ s}^{-1}$ , $t_{1/2} = 1.4 \text{ h}$	$10^{-4} \text{ s}^{-1} \leq k_{298} \leq 10^{-2} \text{ s}^{-1}$ ; $t_{1/2} > 69 \text{ s}$
$[\text{Cu}(\mathbf{3} \ \& \ \mathbf{4})]^+$ (pirouette)	$k_{298} = 0.007 \text{ s}^{-1}$ , $t_{1/2} = 99 \text{ s}$	$k_{298} = 17 \text{ s}^{-1}$ ; $t_{1/2} = 0.04 \text{ s}$
$[\text{Cu}(\mathbf{75} \ \& \ \mathbf{76})]^+$ ( $n = 1$ )	$k_{298} = 5 \text{ s}^{-1}$ , $t_{1/2} = 0.14 \text{ s}$	$k_{298} > 500 \text{ s}^{-1}$ , $t_{1/2} < 1.4 \text{ ms}$
$[\text{Cu}(\mathbf{75} \ \& \ \mathbf{76})]^+$ ( $n = 3$ )	$k_f = 12 \text{ s}^{-1}$ , $t_{1/2} = 0.06 \text{ s}$ ( $-40^\circ\text{C}$ )	$k_b > 1200 \text{ s}^{-1}$ , $t_{1/2} < 0.6 \text{ ms}$ ( $-40^\circ\text{C}$ )
$[\text{Cu}(\mathbf{77} \ \& \ \mathbf{78})]^+$ (shuttle)	$k_{298} = 0.8 \text{ s}^{-1}$ , $t_{1/2} = 0.9 \text{ s}$	$k_{298} = 50 \text{ s}^{-1}$ , $t_{1/2} = 14 \text{ ms}$
$[\text{Cu}(\mathbf{79} \ \& \ \mathbf{80})]^+$ (shuttle)	$k_{298} = 2 \text{ s}^{-1}$ , $t_{1/2} = 0.35 \text{ s}$	$k_{298} > 50 \text{ s}^{-1}$ , $t_{1/2} < 14 \text{ ms}$
$[\text{Zn}(\mathbf{18})]^{2+} + \mathbf{85}$ and $[\text{Cu}(\mathbf{85})]^+ + \mathbf{18}$	$k_{298} = 4.3 \times 10^{-3} \text{ s}^{-1}$ , $t_{1/2} = 161 \text{ s}$ ( $\text{Zn}^{2+}$ )	$k_{298} = 6.8 \times 10^{-3} \text{ s}^{-1}$
$[\text{Cu}(\mathbf{81} \ \& \ \mathbf{82})]^+$ (pirouette)	$k_{298} = 620 \text{ s}^{-1}$ , $t_{1/2} < 1.1 \text{ ms}$ in $\text{CH}_2\text{Cl}_2$	–
$[\text{Cu}(\mathbf{83} \ \& \ \mathbf{84})]^+$ (shuttle)	$k_{298} = 2 \text{ s}^{-1}$	–

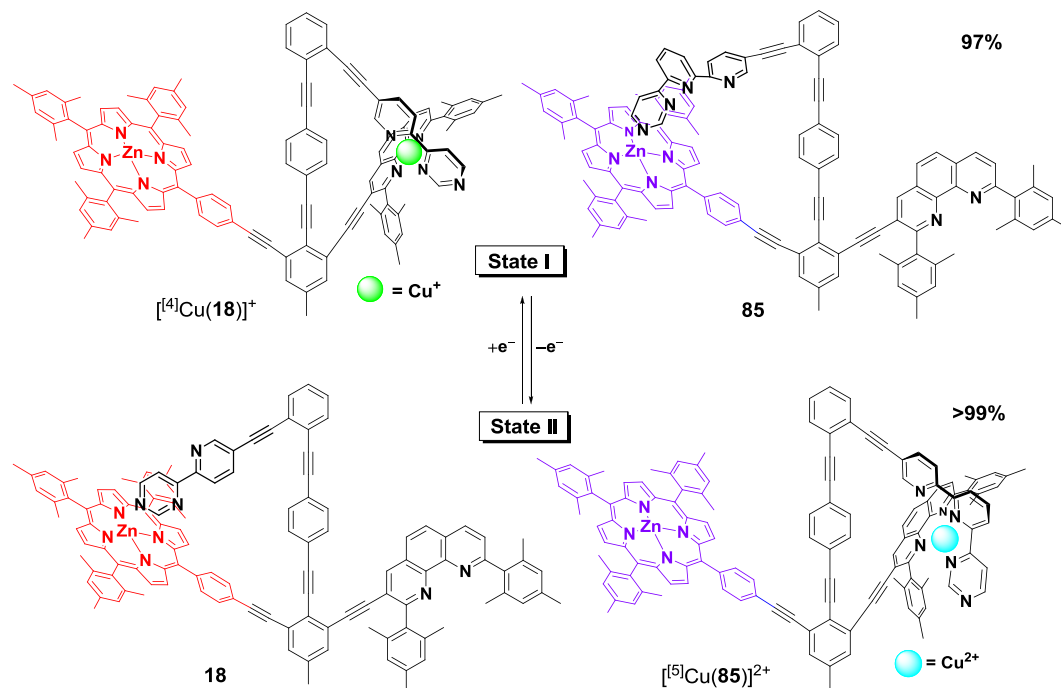


Fig. 39. Intermolecular communication between two nanoswitches [95].

centration of the receiver nanoswitch **85**, the rate-limiting step most likely involves opening of the zinc-loaded nanoswitch prior to metal ion transfer. The reverse process, however, could be monitored with copper being transmitted. Upon combining switch **18** with  $[\text{Cu}(\mathbf{85})]^+$ , the copper(I) ion translocation occurred with a half-time  $t_{1/2} = 102$  s at 25 °C ( $k_{298} = 6.8 \times 10^{-3} \text{ s}^{-1}$ ,  $\text{CH}_2\text{Cl}_2$ ) producing  $[\text{Cu}(\mathbf{18})]^+$  and **85** [95].

Slow metal translocation on the min timescale was equally seen in a redox-actuated switching of  $[\text{Cu}(\mathbf{18})(\mathbf{53})]^+$  [33] (for ligand **53**, see Fig. 25). After one-electron oxidation at the ferrocenyl group using **TBA** (**63**), phenanthroline  $\mathbf{53}^+$  dissociated from the intermolecular copper complex and the arm toggled fully around within 7 min generating  $[\text{Cu}(\mathbf{18})]^+$ . Reduction with decamethylferrocene (**64**) generated  $[\text{Cu}(\mathbf{18})(\mathbf{53})]^+$  within 2 min. These examples of slow ligand dissociation fall into the same kinetic region as the early shuttle motions by Sauvage.

Another experiment demonstrated that the dissociation of a phenanthroline from the copper(I) center is rather slow (see Fig. 40) [38]. The dicopper nanoswitch  $[\text{Cu}_2(\mathbf{86})]^{2+}$  was investigated by variable temperature (VT) <sup>1</sup>H NMR spectra in 1,1,2,2-

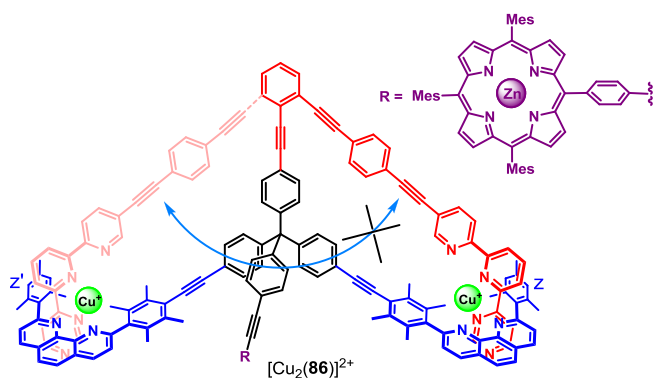


Fig. 40. Exchange of the terpy arm does not occur between the two copper(I) phenanthroline sites in  $[\text{Cu}(\mathbf{86})_2]^{2+}$  [38].

tetrachloroethane- $\text{D}_2$ , but no coalescence of protons z-H at the HETTAP complex at 6.29 ppm and protons z'-H at the coordinatively frustrated copper(I)-loaded phenanthroline station at 7.01 ppm was observed in the temperature range 298–373 K. Moreover, attempts to initiate spontaneous toggling by adding nucleophiles such as acetonitrile  $d_3$  and 4-iodopyridine failed.

#### 4.4. Supramolecular machines

While the strategic work of Sauvage on improving the motional speed in rotaxanes and catenanes has addressed various factors to facilitate  $N,N_{\text{phen}} \rightarrow [{}^{\text{I}}\text{Cu}(\text{phen})]^{2+}$  and  $N,N,N_{\text{terpy}} \rightarrow [{}^{\text{I}}\text{Cu}(\text{phen})]^+$  bond dissociation (Chapter 4.2), even faster motions in supramolecular switches and machinery are possible when the much more facile  $N_{\text{py}} \rightarrow [\text{Cu}(\text{phen})]^+$  bond cleavage is implemented. As with any other examples, though, the rate constant will again depend on the individual mechanistic scenario, which often is not rigorously elucidated. Equally, none of the studies has systematically sought to investigate the influence of nucleophiles on rates although reports from three decades ago already clearly indicated that this is an important factor [72]. Kume' and Nishihara's analysis of the tristate rotor  $[\text{Cu}(\mathbf{31})(\mathbf{35})]^+$  (Fig. 41) resulted in rate constants in the order of 4–40 s<sup>-1</sup> that were assigned to a single  $N_{\text{py}} \rightarrow [\text{Cu}(\text{phen})]^+$  bond cleavage, because the mechanism should involve rotation of the pyridine or the pyrimidine ring about the pyridine-pyrimidine axis [53]. In the transition state, the  $N_{\text{py}} \rightarrow [\text{Cu}(\text{phen})]^+$  bond is cleaved and additionally delocalization between the two orthogonal heterocyclic ring systems is destroyed. Unexpectedly, these rate constants are in the same ballpark as those for some of the faster pirouetting and shuttling events in rotaxanes although the latter formally require a rate-determining  $N,N_{\text{phen}} \rightarrow [{}^{\text{I}}\text{Cu}(\text{phen})]^{2+}$  bond scission.

A detailed investigation addressed the dynamics of the copper(I) pyridylpyrimidine rotor system in the heteroleptic complex  $[\text{Cu}(\mathbf{32})(\text{dppp})]^+$  (dppp = 1,3-bis(diphenylphosphino)propane) [96]. Here, the solvent dependence of the thermal equilibration rate constant was even more pronounced ( $\text{CD}_2\text{Cl}_2$ :  $k_{298} = 20 \text{ s}^{-1}$ ;  $\text{CDCl}_3$ :

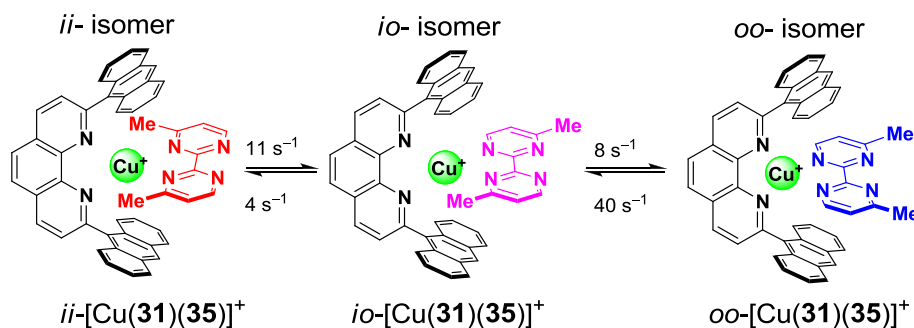


Fig. 41. A trisate rotor [53].

$k_{298} = 50 \text{ s}^{-1}$ ; acetone  $d_6$ :  $k_{298} = 200 \text{ s}^{-1}$ ;  $\text{CD}_3\text{CN}$ :  $k_{298} = 500 \text{ s}^{-1}$  than in  $[\text{Cu}(\mathbf{32})(\mathbf{34})]^+$ .

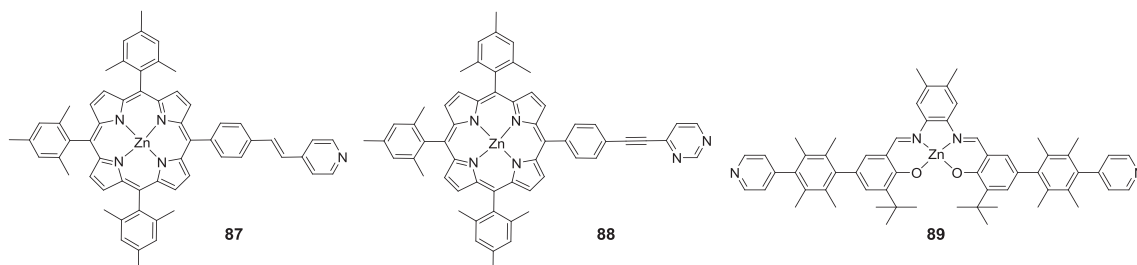
A large body of data became accessible from the VT NMR analysis of multi-component rotors as those depicted in Figs. 22 and 23. While the original expectation was that the barrier of rotation would increase linearly with the number of  $N_{\text{py}} \rightarrow [\text{Cu}(\text{phen})]^+$  bond cleavage reactions in the rate-determining step, the detailed analysis furnished a much more intricate picture. Contributors to the activation barrier are not only the number of coordinative interactions but also large attractive dispersive forces between the departing pyridine ligands and the large aromatic units in the 2- and 9-positions of the phenanthroline. Another issue of great importance is strain. Depending on the design, the rotors experience full strain release in the departure step. Finally, the presence of spurious traces of nucleophiles is expected to influence the rate. For instance, in most examples, acetonitrile is present, usually due to the use of  $[\text{Cu}(\text{MeCN})_4]^+$  as a source for copper. In

those cases, rigorous removal of acetonitrile changed the rates significantly [63]. As such the kinetic data can be influenced by number of contributors.

The rate constants in Table 4 (nanorotors) may be compared with the rate constant of the intermolecular and unimpeded self-exchange in  $[\text{Cu}(\mathbf{90})(\mathbf{91})]^+ + [\text{Cu}(\mathbf{90})]^+$ :  $k_{298} = 1.5 \times 10^8 \text{ s}^{-1}$  (Fig. 42) [63]! The barrier for this  $N_{\text{py}} \rightarrow [\text{Cu}(\text{phen})]^+$  bond cleavage ( $\Delta G_{298}^\ddagger = 26.5 \text{ kJ mol}^{-1}$ ) is much lower than the barrier of rotational exchange in **ROT-5** =  $[\text{Cu}_4(\mathbf{43})(\mathbf{46})(\text{DABCO})]^{4+}$  ( $\Delta G_{298}^\ddagger = 48.3 - \text{kJ mol}^{-1}$ ). The identical setting about the coordination site to be cleaved in  $[\text{Cu}(\mathbf{90})(\mathbf{91})]^+$  and in **ROT-5** (Fig. 23) and the notable differential barrier  $\Delta\Delta G_{298}^\ddagger = 21.8 \text{ kJ mol}^{-1}$  point to huge effects hampering the motion in the nanorotors, possibly due to the restricted trajectory of departure in the intramolecular system. The comparison of the single-pyridine rotor  $[\text{Cu}_2(\mathbf{40})(\mathbf{87})(\text{DABCO})]^{2+}$  with  $[\text{Cu}(\mathbf{90})(\mathbf{91})]^+ + [\text{Cu}(\mathbf{90})]^+$  even identifies a rate acceleration in the order of 300,000.

Table 4

Rate constants from some selected nanorotors.



Nanorotor	Comments	Cleavage of $N_{\text{py}} \rightarrow [^{141}\text{Cu}]^+$
$[\text{Cu}_4(\mathbf{43})(\mathbf{46})(\text{DABCO})]^{4+}$	Single pyridine rotator, strained	$k_{298} = 22\,000 \text{ s}^{-1}$ ( $t_{1/2} = 30 \mu\text{s}$ ) [63]
$[\text{Cu}_2(\mathbf{40})(\mathbf{87})(\text{DABCO})]^{2+}$	Single pyridine rotator, strainfree	$k_{298} = 500 \text{ s}^{-1}$ ( $t_{1/2} = 1.4 \text{ ms}$ ) [97]
$[\text{Cu}_2(\mathbf{40})(\mathbf{43})(\text{DABCO})]^{2+}$	Single pyridine rotator, strained	$k_{298} = 20\,000 \text{ s}^{-1}$ ( $t_{1/2} = 35 \mu\text{s}$ ) [96]
$[\text{Cu}_2(\mathbf{40})(\mathbf{88})(\text{DABCO})]^{2+}$	Single pyrimidine rotator, strained	$k_{298} = 42\,000 \text{ s}^{-1}$ ( $t_{1/2} = 17 \mu\text{s}$ ) [96]
$[\text{Cu}_4(\mathbf{39})(\mathbf{89})(\text{DABCO})]^{4+}$	5,15-Di-pyridinesalphen, strained	$k_{298} = 0.2 \text{ s}^{-1}$ ( $t_{1/2} = 3.4 \text{ s}$ ) [98]
$[\text{Cu}_4(\mathbf{41})(\mathbf{46})(\text{DABCO})]^{4+}$	5,10-Di-pyridine rotator, strained	$k_{298} = 0.4 \text{ s}^{-1}$ ( $t_{1/2} = 1.7 \text{ s}$ ) [63]
$[\text{Cu}_4(\mathbf{44})(\mathbf{46})(\text{DABCO})]^{4+}$	5,15-Di-pyridine rotator, strained	$k_{298} = 380 \text{ s}^{-1}$ ( $t_{1/2} = 1.8 \text{ ms}$ ) [63]
$[\text{Cu}_4(\mathbf{45})(\mathbf{46})(\text{DABCO})]^{4+}$	5,10,15-Tri-pyridine rotator, strained	$k_{298} \ll 0.1 \text{ s}^{-1}$ [63]

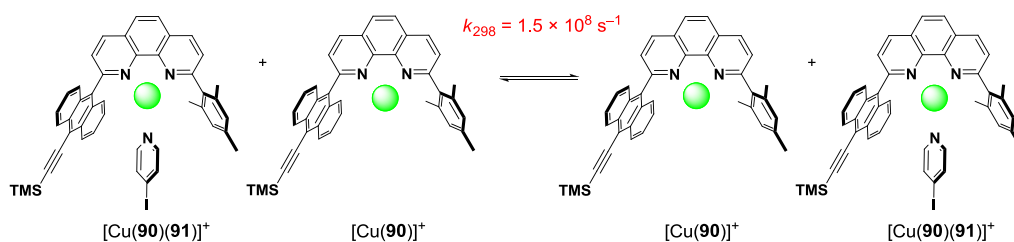
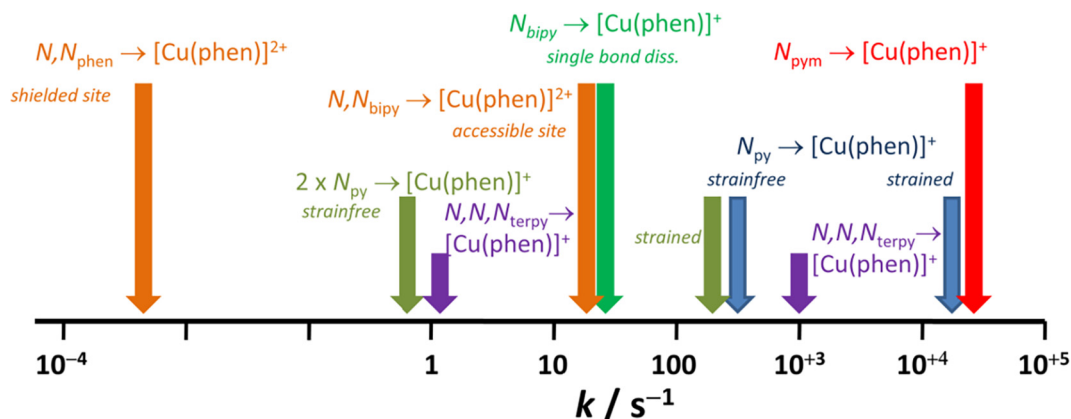
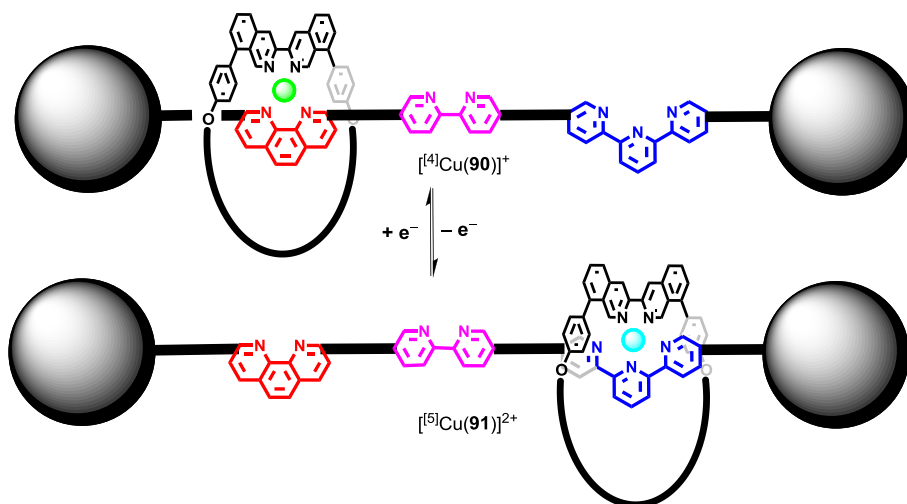


Fig. 42. Rapid self-exchange observed in intermolecular ligand exchange [63].





**Fig. 43.** Summary of intramolecular rate constants ( $N,N$  = dissociation of chelate ligand;  $N$  = dissociation of one nitrogen donor atom). The rate constant for the intermolecular  $N_{py} \rightarrow [Cu(phen)]^+$  bond cleavage is outside of the depicted range ( $k_{298} = 1.5 \times 10^6 \text{ s}^{-1}$ , see Fig. 42).



**Fig. 44.** Shuttling along a thread with three stations [99].

#### 4.5. Conclusions on kinetic data

Due to the limited material and the lack of explicit mechanistic scenarios the interpretation of the kinetic data cannot be conclusive. If we screen the various kinetically analyzed processes the most defined ones are those ignited either by oxidation/reduction or pure thermal exchange reactions. Other processes that were triggered by addition of a second metal ion are quite complex, see Fig. 6, with the consequence that the true rate-determining step often is not known. Taking the kinetic data in Tables 1–4 into account one can come up with a graphical depiction (Fig. 43) that illustrates the rough trend.

Although the data in Fig. 43 convey some guidelines how to equip switches or machines with rapidly moving elements, the field of machine-like molecular entities is still full of unforeseen surprises. While we have focused on the ligand – copper bond cleavage as the usual rate determining step, a study by Sauvage has revealed surprising insight about the usefulness of intermediate stations for speeding up shuttling [99]. The presence of an intermediate 2,2'-bipyridine group in **90** was claimed to speed up the shuttling of the macrocycle between the phenanthroline and the terpyridine station. At present the effect is not fully understood. The bipyridine group may behave as a real “station”, hosting the mobile macrocycle for some short time, or its function is merely to modify the nature of the axis. In any case, such observations clearly indicate that long-distance motions on a thread may

require the fine-tuning of additional parameters aside of the ligand – copper bond cleavage (see Fig. 44).

## 5. Conclusion

The fascinating arena of molecular machines, switches and devices is not only a playground for establishing new nanomechanical functions, but it is also an area in which physical (in)organic chemistry finds new challenges. The present survey demonstrates the eminent importance of various dynamic interactions  $N_L \rightarrow [Cu(phen)]^+$  ( $N_L = \text{terpy, phen, py}$ ) for equipping molecular devices with motion. The rate constants for each of these interactions vary over a wide range, for instance, in the case of the  $N_{py} \rightarrow [Cu(phen)]^+$  interaction the rates differ by >5 orders of magnitude. Clearly, the design of future devices will require additional and more detailed structure–reactivity (= rate) relationships for optimization of nanomechanical machine functions.

## Acknowledgments

The authors are indebted to the Deutsche Forschungsgemeinschaft for generous funding in the area of nanoswitches (DFG 647/19-2) and nanorotors (DFG 647/20-1).

## References

- [1] J.-P. Sauvage, From chemical topology to molecular machines (nobel lecture), *Angew. Chem. Int. Ed.* 56 (2017) 11080–11093.
- [2] C.O. Dietrich-Buchecker, J.-P. Sauvage, J.-P. Kintzinger, Une nouvelle famille de molécules: les metallo-catenanes, *Tetrahedron Lett.* 24 (1983) 5095–5098.
- [3] J.-P. Collin, C. Dietrich-Buchecker, P. Gaviña, M.C. Jimenez-Molero, J.-P. Sauvage, Shuttles and muscles: linear molecular machines based on transition metals, *Acc. Chem. Res.* 34 (2001) 477–487.
- [4] C.O. Dietrich-Buchecker, J.-P. Sauvage, A synthetic molecular trefoil knot, *Angew. Chem. Int. Ed. Engl.* 28 (1989) 189–192.
- [5] J.P. Sauvage, Interlacing molecular threads on transition metals: catenands, catenanes, and knots, *Acc. Chem. Res.* 23 (1990) 319–327.
- [6] A. Livoreil, C.O. Dietrich-Buchecker, J.-P. Sauvage, Electrochemically triggered swinging of a [2]-catenate, *J. Am. Chem. Soc.* 116 (1994) 9399–9400.
- [7] M. Denis, S.M. Goldup, The active template approach to interlocked molecules, *Nat. Rev. Chem.* 1 (2017) 0061.
- [8] D.R. Kohn, L.D. Movsisyan, A.L. Thompson, H.L. Anderson, Porphyrin-polyene [3]- and [5]rotaxanes, *Org. Lett.* 19 (2017) 348–351.
- [9] S. Saito, Synthesis of interlocked compounds utilizing the catalytic activity of macrocyclic phenanthroline-Cu complexes, *J. Incl. Phenom. Macrocycl. Chem.* 82 (2015) 437–451.
- [10] J.E. Beves, B.A. Blight, C.J. Campbell, D.A. Leigh, R.T. McBurney, Strategies and tactics for the metal-directed synthesis of rotaxanes, knots, catenanes, and higher order links, *Angew. Chem. Int. Ed.* 50 (2011) 9260–9327.
- [11] J.-P. Sauvage, Transition metal-complexed catenanes and rotaxanes as molecular machine prototypes, *Chem. Commun.* (2005) 1507–1510.
- [12] N. Armaroli, V. Balzani, J.-P. Collin, P. Gaviña, J.-P. Sauvage, B. Ventura, Rotaxanes incorporating two different coordinating units in their thread: synthesis and electrochemically and photochemically induced molecular motions, *J. Am. Chem. Soc.* 121 (1999) 4397–4408.
- [13] L. Raehm, J.-M. Kern, J.-P. Sauvage, A transition metal containing rotaxane in motion: electrochemically induced pirouetting of the ring on the threaded dumbbell, *Chem. Eur. J.* 5 (1999) 3310–3317.
- [14] M.C. Jiménez, C. Dietrich-Buchecker, J.-P. Sauvage, Towards synthetic molecular muscles: contraction and stretching of a linear rotaxane dimer, *Angew. Chem. Int. Ed.* 39 (2000) 3284–3287.
- [15] C.J. Bruns, J.F. Stoddart, Rotaxane-based molecular muscles, *Acc. Chem. Res.* 47 (2014) 2186–2199.
- [16] A. Joosten, Y. Trolez, J.-P. Collin, V. Heitz, J.-P. Sauvage, Copper(I)-assembled 3rotaxane whose two rings act as flapping wings, *J. Am. Chem. Soc.* 134 (2012) 1802–1809.
- [17] A. El-ghayouy, A. Harriman, A.D. Cian, J. Fischer, R. Ziessel, Redox cycling of segmented copper helicenes, *J. Am. Chem. Soc.* 120 (1998) 9973–9974.
- [18] F. Niess, V. Duplan, J.-P. Sauvage, Interconversion between a vertically oriented transition metal-complexed figure-of-eight and a horizontally disposed one, *J. Am. Chem. Soc.* 136 (2014) 5876–5879.
- [19] J.J. Davis, G.A. Orlowski, H. Rahman, P.D. Beer, Mechanically interlocked and switchable molecules at surfaces, *Chem. Commun.* 46 (2010) 54–63.
- [20] N. Weber, C. Hamann, J.-M. Kern, J.-P. Sauvage, Synthesis of a copper [3] rotaxane able to function as an electrochemically driven oscillatory machine in solution, and to form SAMs on a metal surface, *Inorg. Chem.* 42 (2003) 6780–6792.
- [21] L. Raehm, J.-M. Kern, J.-P. Sauvage, C. Hamann, S. Palacin, J.-P. Bourgoin, Disulfide- and thiol-incorporating copper catenanes: synthesis, deposition onto gold, and surface studies, *Chem. Eur. J.* 8 (2002) 2153–2162.
- [22] S. Zahn, W. Reckien, B. Kirchner, H. Staats, J. Matthey, A. Lützen, Towards allosteric receptors: adjustment of the rotation barrier of 2,2'-bipyridine derivatives, *Chem. Eur. J.* 15 (2009) 2572–2580.
- [23] P.D. Beer, A.S. Rothin, A new allosteric bis crown ether ligand that displays negative binding co-operativity of the biquat dication by the complexation of a transition metal guest, *J. Chem. Soc., Chem. Commun.* (1988) 52–54.
- [24] H. Staats, F. Eggers, O. Haß, F. Fahrenkrug, J. Matthey, U. Lünig, A. Lützen, Towards allosteric receptors – synthesis of resorcinarene-functionalized 2,2'-bipyridines and their metal complexes, *Eur. J. Org. Chem.* (2009) 4777–4792.
- [25] H. Staats, A. Lützen, Size selective recognition of small esters by a negative allosteric hemiacerand, *Beilstein J. Org. Chem.* 6 (2010) 10.
- [26] H.-G. Weinig, R. Krauss, M. Seydack, J. Bendig, U. Koert, Molecular signal transduction by conformational transmission: use of tetrasubstituted perhydroanthracenes as transducers, *Chem. Eur. J.* 7 (2001) 2075–2088.
- [27] M.H. Al-Sayah, R. McDonald, N.R. Branda, Structural studies on hydrogen-bonding receptors for barbiturate guests that use metal ions as allosteric inhibitors, *Eur. J. Org. Chem.* (2004) 173–182.
- [28] I.O. Fritsky, R. Ott, R. Krämer, Allosteric regulation of artificial phosphoesterase activity by metal ions, *Angew. Chem. Int. Ed.* 39 (2000) 3255–3258.
- [29] G. Haberhauer, Control of planar chirality: the construction of a copper-ion-controlled chiral molecular hinge, *Angew. Chem. Int. Ed.* 47 (2008) 3635–3638.
- [30] G. Haberhauer, A metal-ion-driven supramolecular chirality pendulum, *Angew. Chem. Int. Ed.* 49 (2010) 9286–9289.
- [31] M. Schmittel, A. Ganz, Stable mixed phenanthroline copper(I) complexes. Key building blocks for supramolecular coordination chemistry, *Chem. Commun.* (1997) 999–1000.
- [32] M. Schmittel, S. Pramanik, S. De, A reversible nanoswitch as an ON-OFF photocatalyst, *Chem. Commun.* 48 (2012) 11730–11732.
- [33] M. Schmittel, S. De, S. Pramanik, Redox-dependent self-sorting toggles a rotary nanoswitch, *Org. Biomol. Chem.* 13 (2015) 8937–8944.
- [34] S. De, S. Pramanik, M. Schmittel, A monomer-dimer nanoswitch that mimics the working principle of the SARS-CoV 3CLpro enzyme controls copper-catalysed cyclopropanation, *Dalton Trans.* 43 (2014) 10977–10982.
- [35] J. Shi, J. Sivaraman, J. Song, Mechanism for controlling the dimer-monomer switch and coupling dimerization to catalysis of the severe acute respiratory syndrome coronavirus 3C-like protease, *J. Virol.* 82 (2008) 4620–4629.
- [36] S. Gaikwad, A. Goswami, S. De, M. Schmittel, A metalloregulated four-state nanoswitch controls two-step sequential catalysis in an eleven-component system, *Angew. Chem. Int. Ed.* 55 (2016) 10512–10517.
- [37] S. De, S. Pramanik, M. Schmittel, A toggle nanoswitch alternately controlling two catalytic reactions, *Angew. Chem. Int. Ed.* 53 (2014) 14255–14259.
- [38] S. Gaikwad, M. Schmittel, Five-state rotary nanoswitch, *J. Org. Chem.* 82 (2017) 343–352.
- [39] D. Zhao, T. van Leeuwen, J. Cheng, B.L. Feringa, Dynamic control of chirality and self-assembly of double-stranded helicates with light, *Nat. Chem.* 9 (2017) 250–256.
- [40] A. Faulkner, T. van Leeuwen, B.L. Feringa, S.J. Wezenberg, Allosteric regulation of the rotational speed in a light-driven molecular motor, *J. Am. Chem. Soc.* 138 (2016) 13597–13603.
- [41] M.L. Saha, M. Schmittel, Degree of molecular self-sorting in multicomponent systems, *Org. Biomol. Chem.* 10 (2012) 4651–4684.
- [42] Z. He, W. Jiang, C.A. Schalley, Integrative self-sorting: a versatile strategy for the construction of complex supramolecular architecture, *Chem. Soc. Rev.* 44 (2015) 779–789.
- [43] V.E. Campbell, X. de Hatten, N. Delsuc, B. Kauffmann, I. Huc, J.R. Nitschke, Cascading transformations within a dynamic self-assembled system, *Nat. Chem.* 2 (2010) 684–687.
- [44] M.L. Saha, S. Pramanik, M. Schmittel, Spontaneous and catalytic fusion of supramolecules, *Chem. Commun.* 48 (2012) 9459–9461.
- [45] N. Mittal, M.L. Saha, M. Schmittel, Fully reversible three-state interconversion of metallosupramolecular architectures, *Chem. Commun.* 52 (2016) 8749–8752.
- [46] M.L. Saha, M. Schmittel, Metal-ligand exchange in a cyclic array: the stepwise advancement of supramolecular complexity, *Inorg. Chem.* 55 (2016) 12366–12375.
- [47] A. Adamski, M. Osińska, M. Kubicki, Z. Hnatejko, G. Consiglio, V. Patroniak, Molecular switching of copper complexes with quaterpyridine, *Eur. J. Inorg. Chem.* (2017) 859–872.
- [48] K. Nomoto, S. Kume, H. Nishihara, A single molecular system gating electron transfer by ring inversion of a methylpyridylpyrimidine ligand on copper, *J. Am. Chem. Soc.* 131 (2009) 3830–3831.
- [49] S. Kume, K. Nomoto, T. Kusamoto, H. Nishihara, Intramolecular electron arrangement with a rotative trigger, *J. Am. Chem. Soc.* 131 (2009) 14198–14199.
- [50] S. Kume, H. Nishihara, Synchronized motion and electron transfer of a redox-active rotor, *Dalton Trans.* 40 (2011) 2299–2305.
- [51] M. Nishikawa, Y. Takara, Y. Hattori, K. Nomoto, T. Kusamoto, S. Kume, H. Nishihara, Structural modification on Copper(I)-pyridylpyrimidine complexes for modulation of rotational dynamics, redox properties, and phototriggered isomerization, *Inorg. Chem.* 52 (2013) 8962–8970.
- [52] M. Nishikawa, K. Nomoto, S. Kume, K. Inoue, M. Sakai, M. Fujii, H. Nishihara, Dual emission caused by ring inversion isomerization of a 4-methyl-2-pyridylpyrimidine copper(I) complex, *J. Am. Chem. Soc.* 132 (2010) 9579–9581.
- [53] Y. Takara, T. Kusamoto, T. Masui, M. Nishikawa, S. Kume, H. Nishihara, A single-molecular twin rotor: correlated motion of two pyrimidine rings coordinated to copper, *Chem. Commun.* 51 (2015) 2896–2898.
- [54] K.A. McNitt, K. Parimal, A.I. Share, A.C. Fahrenbach, E.H. Witlicki, M. Pink, D.K. Bediako, C.L. Plaisier, N. Le, L.P. Heeringa, D.A.V. Griend, A.H. Flood, Reduction of a redox-active ligand drives switching in a Cu(I) pseudorotaxane by a bimolecular mechanism, *J. Am. Chem. Soc.* 131 (2009) 1305–1313.
- [55] A.I. Share, K. Parimal, A.H. Flood, Bilability is defined when one electron is used to switch between concerted and stepwise pathways in Cu(I)-based bistable [2/3]pseudorotaxanes, *J. Am. Chem. Soc.* 132 (2010) 1665–1675.
- [56] C.R. Benson, A.I. Share, M.G. Marzo, A.H. Flood, Double switching of two rings in palindromic [3] pseudorotaxanes, *Inorg. Chem.* 55 (2016) 3767–3776.
- [57] S.K. Samanta, A. Rana, M. Schmittel, Reversible cargo shipping between orthogonal stations of a nanoscaffold upon redox input, *Dalton Trans.* 43 (2014) 9438–9447.
- [58] S. Neogi, G. Schnakenburg, Y. Lorenz, M. Engeser, M. Schmittel, Implications of stoichiometry-controlled structural changeover between heteroleptic trigonal [Cu(phenAr<sub>2</sub>)(py)]<sup>+</sup> and tetragonal [Cu(phenAr<sub>2</sub>)(py)<sub>2</sub>]<sup>+</sup> motifs for solution and solid-state supramolecular self-assembly, *Inorg. Chem.* 51 (2012) 10832–10841.
- [59] M. Schmittel, B. He, J. Fan, J.W. Bats, M. Engeser, M. Schlosser, H.-J. Deiseroth, Cap for copper(I) ions! metallosupramolecular solid and solution state structures on the basis of the dynamic tetrahedral Cu(phenAr<sub>2</sub>)(py)<sub>2</sub><sup>+</sup> motif, *Inorg. Chem.* 48 (2009) 8192–8200.
- [60] S.K. Samanta, M. Schmittel, Four-component supramolecular nanorotors, *J. Am. Chem. Soc.* 135 (2013) 18794–18797.
- [61] S.K. Samanta, J.W. Bats, M. Schmittel, A five-component nanorotor with speed regulation, *Chem. Commun.* 50 (2014) 2364–2366.

- [62] S.K. Samanta, A. Rana, M. Schmittel, Conformational slippage determines rotational frequency in five-component nanorotors, *Angew. Chem. Int. Ed.* 55 (2016) 2267–2272.
- [63] P.K. Biswas, S. Saha, Y. Nanaji, A. Rana, M. Schmittel, Influence of rotator design on the speed of self-assembled four-component nanorotors: coordinative versus dispersive interactions, *Inorg. Chem.* 56 (2017) 6662–6670.
- [64] M. Schmittel, S. De, S. Pramanik, Reversible ON/OFF nanoswitch for organocatalysis: mimicking the locking and unlocking operation of CaMKII, *Angew. Chem. Int. Ed.* 51 (2012) 3832–3836.
- [65] H. Schulman, The multifunctional Ca<sup>2+</sup>/calmodulin-dependent protein kinases, *Curr. Opin. Chem. Biol.* 5 (1993) 247–253.
- [66] N. Mittal, S. Pramanik, I. Paul, S. De, M. Schmittel, Networking nanoswitches for ON/OFF control of catalysis, *J. Am. Chem. Soc.* 139 (2017) 4270–4273.
- [67] S. Gaikwad, S. Pramanik, S. De, M. Schmittel, A high-speed network of nanoswitches for on/off control of catalysis, *Dalton Trans.* 47 (2018) 1786–1790.
- [68] A. Goswami, S. Pramanik, M. Schmittel, Catalytically active nanorotor reversibly self-assembled by chemical signaling within an eight-component network, *Chem. Commun.* 54 (2018) 3955–3958.
- [69] L. Helm, A.E. Merbach, Water exchange on metal ions: experiments and simulations, *Coord. Chem. Rev.* 187 (1999) 151–181.
- [70] P.T. Corbett, J. Leclaire, L. Vial, K.R. West, J.-L. Wietor, J.K.M. Sanders, S. Otto, Dynamic combinatorial chemistry, *Chem. Rev.* 106 (2006) 3652–3711.
- [71] G.C. van Stein, G. van Koten, B. de Bok, L.C. Taylor, K. Vrieze, C. Brevard, Silver(I) and copper(I) bis(pyridine-2-carbaldehyde-imine) triflate complexes studied in solution by <sup>1</sup>H, <sup>1</sup>H-<sup>109</sup>Ag, INEPT <sup>15</sup>N and INEPT <sup>109</sup>Ag NMR, *Inorg. Chim. Acta* 89 (1984) 29–39.
- [72] U.M. Frei, G. Geier, Lewis-base-catalyzed diimine-ligand-substitution reactions at copper(I), *Inorg. Chem.* 31 (1992) 3132–3137.
- [73] E. Riesgo, Y.-Z. Hu, F. Bouvier, R.P. Thummel, Evaluation of diimine ligand exchange on Cu(I), *Inorg. Chem.* 40 (2001) 2541–2546.
- [74] Database for bond energies: iBond 2.0: <http://ibond.chem.tsinghua.edu.cn/>.
- [75] V. Desvergnès-Breuil, V. Hebbe, C. Dietrich-Buchecker, J.-P. Sauvage, J. Lacour, NMR evaluation of the configurational stability of Cu(I) complexes, *Inorg. Chem.* 42 (2003) 255–257.
- [76] V. Hebbe-Viton, V. Desvergnès, J.J. Jodry, C. Dietrich-Buchecker, J.-P. Sauvage, J. Lacour, Chiral spiro Cu(I) complexes. Supramolecular stereocontrol and isomerisation dynamics by the use of TRISPHAT anions, *Dalton Trans.* (2006) 2058–2065.
- [77] I. Pianet, J.-M. Vincent, Isomerization dynamics in homo- and heterochiral atropisomer copper(I) diimine complexes: a 2D EXSY NMR study, *Inorg. Chem.* 43 (2004) 2947–2953.
- [78] J. Jung, J. Jo, M. Laskar, D. Lee, Stereodynamics of metal-ligand assembly: what lies beneath the “simple” spectral signatures of C<sub>2</sub>-symmetric chiral chelates, *Chem. Eur. J.* 19 (2013) 5156–5168.
- [79] M. Hutin, J. Nitschke, Solvent-tunable inversion of chirality transfer from carbon to copper, *Chem. Commun.* (2006) 1724–1726.
- [80] L. Lemus, J. Guerrero, J. Costamagna, R. Lorca, D.H. Jara, G. Ferraudi, A. Oliver, A. G. Lappin, Resolution and characterization of helicate dimer and trimer complexes of 1,3-bis(9-methyl-1,10-phenanthrolin-2-yl)propane with copper (I), *Dalton Trans.* 42 (2013) 11426–11435.
- [81] N.C. Habermehl, P.M. Angus, N.L. Kilah, L. Norén, A.D. Rae, A.C. Willis, S.B. Wild, Asymmetric transformation of a double-stranded, dicopper(I) helicate containing achiral bis(bidentate) Schiff bases, *Inorg. Chem.* 45 (2006) 1445–1462.
- [82] The exchange of disilver(I) helicates occurred with  $k > 2 \times 10^{-3} \text{ s}^{-1}$  ( $t_{1/2} < 5 \text{ min}$ ).
- [83] Y. Furusho, H. Goto, K. Itomi, H. Katagiri, T. Miyagawa, E. Yashima, Synthesis and optical resolution of a Cu(I) double-stranded helicate with ketimine-bridged tris(bipyridine) ligands, *Chem. Commun.* 47 (2011) 9795–9797.
- [84] P.R. Ashton, C.L. Brown, E.J.T. Chrystal, K.P. Parry, M. Pietraszkiwicz, N. Spencer, J.F. Stoddart, Molecular trains: the self-assembly and dynamic properties of two new catenanes, *Ang. Chem. Int. Ed. Engl.* 30 (1991) 1042–1045.
- [85] U. Létinois-Halbes, D. Hanss, J.M. Beierle, J.-P. Collin, J.-P. Sauvage, A fast-moving [2]rotaxane whose stoppers are remote from the copper complex core, *Org. Lett.* 7 (2005) 5753–5756.
- [86] J.-P. Collin, F. Durolo, J. Lux, J.-P. Sauvage, A copper-based shuttling [2]rotaxane with two bidentate chelates in the axis: steric control of the motion, *New J. Chem.* 34 (2010) 34–43.
- [87] F. Durolo, J. Lux, J.-P. Sauvage, A fast-moving copper-based molecular shuttle: synthesis and dynamic properties, *Chem. Eur. J.* 15 (2009) 4124–4134.
- [88] E. Coronado, P. Gaviña, J. Ponce, S. Tatay, Fast pirouetting motion in a pyridine bisamine-containing copper-complexed rotaxane, *Chem. Eur. J.* 20 (2014) 6939–6950.
- [89] J.-P. Collin, F. Durolo, P. Mobian, J.-P. Sauvage, Pirouetting copper(I)-assembled pseudo-rotaxanes: strong influence of the axle structure on the motion rate, *Eur. J. Inorg. Chem.* (2007) 2420–2425.
- [90] E. Coronado, P. Gaviña, J. Ponce, S. Tatay, Fast redox-triggered shuttling motions in a copper rotaxane based on a phenanthroline-terpyridine conjugate, *Org. Biomol. Chem.* 12 (2014) 7572–7580.
- [91] V. Aucagne, J. Berna, J.D. Crowley, S.M. Goldup, K.D. Hänni, D.A. Leigh, P.J. Lusby, V.E. Ronaldson, A.M.Z. Slawin, A. Viterisi, D.B. Walker, Catalytic “active-metal” template synthesis of [2]rotaxanes, [3]rotaxanes, and molecular shuttles, and some observations on the mechanism of the Cu(I)-catalyzed azide-alkyne 1,3-cycloaddition, *J. Am. Chem. Soc.* 129 (2007) 11950–11963.
- [92] B. Colasson, N. Le Poul, Y. Le Mest, O. Renaud, Electrochemically triggered double translocation of two different metal ions with a ditopic calix[6]arene ligand, *J. Am. Chem. Soc.* 132 (2010) 4393–4398.
- [93] C.J. Chang, Searching for harmony in transition-metal signaling, *Nat. Chem. Biol.* 11 (2015) 744–747.
- [94] C.J. Chang, Bioinorganic life and neural activity, *Acc. Chem. Res.* 50 (2017) 535–538.
- [95] S. Pramanik, S. De, M. Schmittel, Bidirectional chemical communication between nanomechanical switches, *Angew. Chem. Int. Ed.* 53 (2014) 4709–4713.
- [96] M. Nishikawa, K. Nomoto, S. Kume, H. Nishihara, Solvated-ion-pairing-sensitive molecular bistability based on copper(I)-coordinated pyrimidine ring rotation, *Inorg. Chem.* 52 (2013) 369–380.
- [97] P. Biswas, S. Saha, T. Paululat, M. Schmittel, Rotating catalysts are superior: Suppressing product inhibition by anchimeric assistance in four-component catalytic machinery, *J. Am. Chem. Soc.* 140 (2018) 9038–9041.
- [98] M.S. Özer, A. Rana, P.K. Biswas, M. Schmittel, Four-component zinc-porphyrin/zinc-salphen nanorotor, *Dalton Trans.* 46 (2017) 9491–9497.
- [99] J.-P. Collin, F. Durolo, J. Lux, J.-P. Sauvage, A rapidly shuttling copper-complexed [2]rotaxane with three different chelating groups in its axis, *Angew. Chem. Int. Ed.* 48 (2009) 8532–8535.